Accepted Manuscript

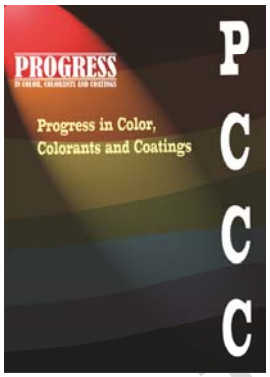

Title: Corrosion Inhibition of Mild Steel in 1 M HCl Using N-benzylidenethiophene-2-sulfonamide: Experimental and Theoretical Investigations

Authors: Hanna H. Al-Doori, Atheer F. Mahmood, Amjed Jumahh, Hasanain Saad Azeez, Raghad. J.Halbos, Ahmed Alamiery, Naseer A. Hussien

Manuscript number**: PCCC-2602-1492**

To appear in: Progresss in Color, Colorants and Coatings

Received: 30 January 2026

Final Revised: 11 May 2026

Accepted: 16 May 2026

Please cite this article as:

H.H. Al-Doori, A.F. Mahmood, A. Jumahh, H. Saad Azeez, R. J. Halbos, A. Alamiery, N.A. Hussien, Corrosion Inhibition of Mild Steel in 1 M HCl Using N-benzylidenethiophene-2-sulfonamide: Experimental and Theoretical Investigations, Prog. Color, Colorants, Coat., 20 (2027) XX-XXX.

DOI: 10.30509/pccc.2026.167764.1492

Corrosion Inhibition of Mild Steel in 1 M HCl Using N-benzylidenethiophene-2-sulfonamide: Experimental and Theoretical Investigations

H.H. Al-Doori[1], A.F. Mahmood[2], A. Jumahh[2], H. Saad Azeez[2], R.J. Halbos[2], A.A. Alamiery [2,3], N.A. Hussien [3]

[1] Al-Karkh University of Science, P.O. Box: 10001, Baghdad, Iraq

[2] University of Technology, P.O. Box: 10001, Baghdad, Iraq

[3] Science and Technology Department, Al-Ayen Iraqi University, AUIQ, P.O. Box: 64001, Thi-Qar, Iraq.

Corresponding author email: dr.ahmed1975@gmail.com

Abstract:

This research investigates the corrosion inhibition performance of a newly developed Schiff base compound, *N-benzylidenethiophene-2-sulfonamide* (NB2S), for protecting mild steel (MS) in a 1 M hydrochloric acid (HCl) environment. A comprehensive evaluation was carried out through various techniques, including weight loss (WL) analysis, electrochemical impedance spectroscopy (EIS), potentiodynamic polarization (PDP), scanning electron microscopy (SEM), and density functional theory (DFT). The mass loss findings indicated that NB2S's inhibitory performance improved with concentration, achieving up to 95.86% efficiency at 0.005 M after a 24-hour immersion. Impedance analysis showed an increase in charge-transfer resistance and a decrease in double-layer capacitance, reflecting strong surface adsorption. PDP measurements revealed that NB2S suppresses cathodic and anodic reactions, acting as a mixed-type inhibitor. Adsorption followed the Langmuir isotherm model, with thermodynamic

parameters indicating a spontaneous, exothermic adsorption process. Computational DFT results aligned with experimental observations, highlighting a low energy gap (ΔE = 5.236 eV), high dipole moment, and electronic features conducive to strong interaction with the metal surface. Surface imaging by SEM further demonstrated formation of a protective barrier on the steel surface.

Keywords: Corrosion inhibition; mild steel; Schiff base; hydrochloric acid; electrochemical impedance spectroscopy; density functional theory.

1. Introduction

Corrosion is a pervasive and costly issue in industries that rely on metals for structural and functional applications. Among industrial materials, Mild steel (MS) is one of the most widely utilized materials because of its mechanical properties, weldability, low cost, and availability. However, it is also highly vulnerable to acidic environments, particularly in acid pickling, oil-well acidizing, and industrial descaling that utilize HCl. In such scenarios, unmitigated corrosion leads to serious degradation of the metal surface, mechanical failure, reduced equipment lifespan, and substantial economic losses [1-3]. To address the persistent issue of metal corrosion, the deployment of inhibitors stands out as an efficient and cost-effective protective strategy. These substances work by forming a protective film over the alloy, effectively isolating it from acids and thereby mitigating the rate of degradation. Among the broad spectrum of inhibitors, organic molecules have garnered considerable interest due to their structural flexibility and strong adsorption capabilities onto metal substrates. This adsorption is typically enhanced by the presence

of heteroatoms such as nitrogen, sulfur, and oxygen, as well as conjugated π-systems, which facilitate coordinated interactions with the steel samples [4-7]. A particularly noteworthy category of organic inhibitors is Schiff base compounds produced through condensation reactions between carbonyl-containing compounds and primary amines, resulting in the formation of imine (−C=N−) linkages. Schiff bases are known for their excellent corrosion-inhibiting behavior, largely due to the availability of lone pair electrons on heteroatoms, which coordinate with unoccupied Fe d-orbitals to establish stable adsorption layers. Their chemical adaptability, ease of synthesis, and potential for environmentally friendly modification make them suitable for corrosion control applications [9-12]. Numerous recent studies have reported Schiff base inhibitors with high efficiencies for steel corrosion in acidic media. However, many of these studies focus primarily on inhibition percentages without sufficiently correlating molecular structure with adsorption mechanism, thermodynamic behavior, and electronic properties. In several cases, inhibitors require relatively high concentrations or show reduced stability at elevated temperatures. Moreover, sulfur-containing Schiff bases remain comparatively underexplored despite sulfur atoms often enhancing adsorption strength through strong interaction with iron surfaces [13-20]. In particular, compounds incorporating both thiophene and sulfonamide functionalities may provide multiple adsorption centers (N, O, S atoms and π-electrons), improving film compactness and interfacial stability. Nevertheless, systematic studies combining weight-loss analysis, electrochemical techniques, surface morphology, adsorption thermodynamics, and density functional theory (DFT) for such systems remain limited. Therefore, the present work investigates N-benzylidenethiophene-2-sulfonamide (NB2S) as a novel sulfur-

containing Schiff base inhibitor for mild steel in 1.0 M HCl, aiming to establish structure–performance relationships and evaluate its practical corrosion protection potential.

2. Experimental

2.1. Materials

Commercially available MS specimens were employed as the working electrodes. These samples were procured from Metal Samples Company and were utilized in both electrochemical and WL assessments. The composition of MS, presented in Table 1, was confirmed by the manufacturer.

Table 1. Elemental composition of MS samples (in weight percent)

C	Mn	Si	Al	S	P	Fe
0.210	0.050	0.380	0.010	0.050	0.090	balance

Prior to every test, the MS specimens were sequentially polished with silicon carbide abrasive papers ranging from 400 to 1200 grit. They were then degreased using acetone, thoroughly rinsed with distilled water, and air-dried at ambient temperature. All surface treatment steps adhered to the ASTM G1-03 standard protocol for metal surface preparation [23, 24].

2.2. Preparation of corrosive medium

A 1.0 M HCl solution was used as the corrosive medium throughout the experiments. It was prepared by accurately diluting 37% HCl (Merck, Malaysia) using deionized water,

following controlled procedures to ensure consistency and reproducibility.

2.3. Weight loss analysis

To assess the inhibitory efficiency of NB2S, weight loss (WL) tests were carried out. MS specimens were immersed in the corrosive medium for varying exposure times 1, 6, 12, and 24 hours under controlled conditions. These tests were performed at four distinct temperatures, 303–343 K, to examine the influence of thermal variation on corrosion behavior. The tests were carried out at varying inhibitor concentrations: 0.000 (blank), 0.001, 0.002, 0.003, 0.004, and 0.005 M. The initial weight of each cleaned and dried specimen was recorded utilizing a highly accurate analytical scale. After immersion in the test solution, coupons were retrieved, thoroughly washed with distilled water followed by acetone, dried at ambient temperature, and weighed again to determine the mass loss. Weight-loss experiments were conducted in triplicate under identical conditions. Reported values represent mean ± standard deviation (n = 3). This method provided quantitative insight into the inhibitor's ability to reduction the variation in C_R with respect to time, temperature, and concentration [23, 24]. The corrosion rate (CR) of the steel samples was calculated using equation 1.

$$C_R = \frac{\omega_0 - \omega_1}{S \times t} \quad (1)$$

where C_R is the rate of corrosion in $mg.h^{-1}.cm^{-2}$, ω_0 and ω_1 are the coupons weights without and with corrosion inhibitor in g, S is the surface area in m^{-2}, and *t* represents the exposed period in h.

Inhibition efficiencies were calculated using equation 2

$$IE\% = \frac{C_{R_0} - C_{R_1}}{C_{R_1}} \times 100\% \quad (2)$$

where C_{R0} and C_{R1} in $mgh^{-1}cm^{-2}$, represent MS corrosion rates without NB2S and with NB2S, respectively. Surface coverage (**θ**) was calculated using equation).

$$\theta = \frac{IE\%}{100} \quad (3)$$

2.4. Thermodynamics

The inhibition mechanism of NB2S on the coupon surface was investigated by examining the adsorption behavior of NB2S using WL measurements of NB2S molecules using WL techniques. The adsorption mode was analyzed through calculation of the free energy (ΔG°_{ads}). Moreover, thermodynamics were studied through WL techniques to further investigate this behavior.

2.5. Electrochemical Testing Procedures

Electrochemical analyses were carried out using a standard three-electrode glass corrosion cell, thermally regulated with a water-jacketed system. The working electrode, composed of MS, had an exposed surface area of 4.5 cm^2. A graphite rod was used as the counter electrode, while a saturated calomel electrode (SCE) served as the reference electrode. Electrolyte solution is 1.0 M HCl, identical to that used in the WL experiments, with and without varying concentrations of NB2S. Before each test, the system was equilibrated for 30 minutes to ensure stabilization of the open circuit potential (OCP). Procedures were performed using a Gamry REF 600 electrochemical workstation, with data collection and analysis managed by the Gamry DC105 and EIS300 software packages. For electrochemical impedance spectroscopy (EIS) measurements, a sinusoidal alternating current (AC) perturbation with an amplitude of 5 mV was applied at the open

circuit potential (OCP) over a frequency range of 100 kHz to 0.1 Hz. The resulting Nyquist and Bode plots were analyzed using appropriate equivalent circuit models. The equivalent circuit consisted of solution resistance (R_s), charge-transfer resistance (R_{ct}), and double-layer capacitance (C_{dl}) [25,26]. EIS, experiments were conducted in triplicate under identical conditions. Reported values represent mean ± standard deviation (n = 3). The inhibitive efficiencies were calculated regarding equation 4,

$$IE\% = \frac{R_{ct} - R_{ct0}}{R_{ct}} \times 100\% \quad (4)$$

where R_{ct0} and R_{ct} represent the charge-transfer resistance values in the absence and presence of NB2S, respectively.

Potentiodynamic polarization (PDP) measurements were performed by sweeping the potential from −200 mV to +200 mV relative to OCP, using a scan rate of 0.5 mV/s. From the resulting polarization curves, key parameters including corrosion current density (I_{corr}), corrosion potential (E_{corr}), and anodic and cathodic Tafel slopes were obtained. These metrics were used to determine IE and identify the inhibitor's behavior as either anodic and/or cathodic. PDP experiments were conducted in triplicate under identical conditions. Reported values represent mean ± standard deviation (n = 3). Inhibition efficiency from polarization data was calculated using equation 5.

$$IE\% = \frac{I_{corr}^{o} - I_{corr}}{I_{corr}^{o}} \times 100\% \quad (5)$$

where I_{corr}^{o} and I_{corr} represent the corrosion current density values in the absence and presence of NB2S, respectively.

2.6. Surface Morphology Analysis

MS specimens were evaluated using Scanning Electron Microscopy (SEM) to assess

corrosion damage and the protective effects of the NB2S inhibitor. The steel samples were immersed in 1.0 M HCl in the absence and presence of NB2S, for a duration of 3 hours. Following exposure, specimens were rinsed with distilled water, dried under ambient conditions, and analyzed using a Hitachi TM1000 Tabletop SEM. Comparative SEM images of treated and untreated surfaces were utilized to qualitatively assess the formation of an inhibitor film and its effectiveness in mitigating surface degradation.

2.7. DFT Calculations

To complement the experimental findings and gain molecular-level insights into interactions between NB2S and MS, Theoretical computations were carried out using Gaussian 03, Revision C.01. Molecular geometry of NB2S was fully optimized employing B3LYP exchange-correlation functional in combination with the 6-31G^{++}(d,p) basis set [27]. All optimizations were carried out without imposing symmetry constraints to ensure the most stable configuration was reached. Key electronic parameters, including the energies of highest occupied and lowest unoccupied molecular orbitals (HOMO and LUMO) respectively, were calculated to evaluate the electron-donating and accepting tendencies of NB2S. The energy gap (ΔE) between these orbitals, representing the reactivity of the molecule, was estimated using Equation (6).

$$\Delta E = E_{LUMO} - E_{HOMO} = IP - EA \qquad (6)$$

where IP and EA represent the ionization potential and electron affinity values respectively.

Based on Koopmans' theorem [28], IP with EA were approximated using equation 7-9.

$$\chi = \frac{IP+EA}{2} \qquad (7)$$

$$\eta = \frac{IP - EA}{2} \quad (8)$$

$$\sigma = \frac{1}{\eta} \quad (9)$$

ΔN which represents the number of electrons transferred from the inhibitor molecule to the MS was estimated based on conceptual DFT principles using equation 10.

$$\Delta N = \frac{\chi_{Fe} - \chi_{inh}}{2(\eta_{Fe} + \eta_{inh})} \quad (10)$$

where χ_{Fe} and χ_{inh} represent the iron electronegativity and corrosion inhibitor electronegativity values respectively.

For these calculations, iron electronegativity (χ_{Fe}) was assumed to be 7.0 eV, and its absolute hardness (η_{Fe}) was taken as zero. These descriptors help predict the reactivity and binding capability of NB2S with the steel surface. Natural Bond Orbital (NBO) analysis was also performed to identify the active adsorption centers and to better understand the electronic interactions responsible for the inhibition mechanism. This was instrumental in identifying active centers responsible for adsorption and inhibition activity [29].

3. Results and Discussion

3.1. WL Analysis

3.1.1. Immersion Time Effect

Influence of concentrations of NB2S on corrosion behavior of MS in 1 M HCl solution was assessed through WL measurements conducted at different exposure periods (1 h, 6 h, 12 h, and 24 h). The data, presented in Figure 1, clearly demonstrate that the C_R decreases significantly with both increasing NB2S concentration and longer immersion times, indicating the effectiveness and persistence of NB2S molecules as protective film

on MS. As shown in Figure 1, the C_R of MS in the uninhibited acid solution (blank) was highest across all immersion times, with values ranging from 7.14 to 7.73 $mg \cdot h^{-1} \cdot cm^{-2}$. Upon the introduction of NB2S at a low concentration of 0.001 M, the C_R dropped significantly to 2.96 $mg \cdot h^{-1} \cdot cm^{-2}$ after 1 hour, corresponding to an inhibition efficiency (IE%) of 58.54%. This trend continued with increasing NB2S concentrations, demonstrating a dose-dependent inhibition effect. At 0.002 M, the C_R further decreased to 1.88 $mg \cdot h^{-1} \cdot cm^{-2}$, with IE% rising to 73.66%. At 0.003 M, the C_R was reduced to nearly one-sixth of the uninhibited value (1.11 $mg \cdot h^{-1} \cdot cm^{-2}$), with IE% reaching 84.45%. The highest inhibition efficiencies were observed at concentrations of 0.004 M and 0.005 M, where C_R values were as low as 0.69 and 0.52 $mg \cdot h^{-1} \cdot cm^{-2}$ respectively, corresponding to IE% values of 90.33% and 92.71% at 1 h. These results clearly establish that the inhibition efficiency of NB2S increases with concentration, likely due to enhanced surface coverage and stronger adsorption of inhibitor molecules on the MS surface. At higher concentrations, a more compact and stable inhibitor film is formed, effectively blocking the active corrosion sites and preventing further dissolution of the metal.

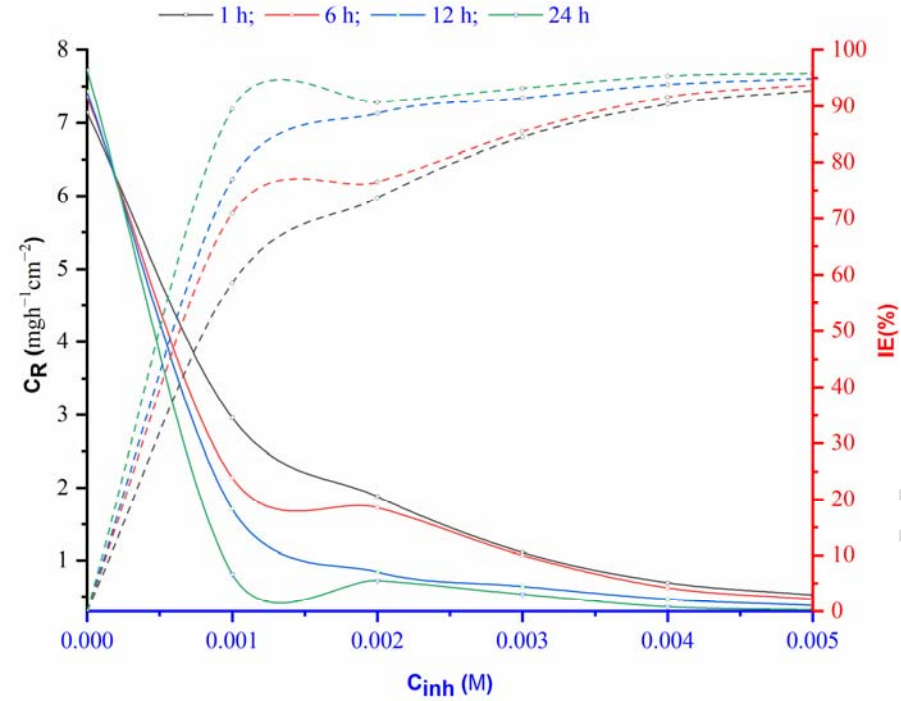

Figure 1. Corrosion rate (C_R) of mild steel (MS) in 1.0 M HCl as a function of immersion time (1, 6, 12, and 24 h) in the absence and presence of NB2S (0.001–0.005 M) at 303 K, obtained from weight-loss measurements.

Immersion time significantly improved the inhibition performance of NB2S. For all concentrations, corrosion rate decreased while inhibition efficiency increased with time, indicating progressive adsorption and stabilization of the protective layer on the mild steel surface. The highest efficiency (95.86%) was obtained at 0.005 M after 24 h, confirming the strong and persistent protective action of NB2S in acidic medium. [30].

3.1.2. Temperature effect

Temperature is a crucial factor influencing both the corrosion behavior of metals and the performance of corrosion inhibitors. Figure 2 presents the C_Rs and corresponding inhibition efficiencies (IE%) of NB2S at various concentrations (0.001–0.005 M) across a temperature range from 303 K to 333 K. The results indicate a strong correlation between temperature, inhibitor concentration, and corrosion inhibition performance. In general,

the C_R of MS tends to increase with temperature due to the acceleration of electrochemical reactions and higher mobility of aggressive ions like Cl^- in acidic environments. However, the presence of NB2S significantly mitigates this effect, especially at higher concentrations. For example, at the lowest inhibitor concentration (0.001 M), the CR decreased from 2.14 $mg \cdot h^{-1} \cdot cm^{-2}$ at 303 K to 1.34 $mg \cdot h^{-1} \cdot cm^{-2}$ at 333 K, but the corresponding IE% increased from 70.92% to 89.52%. This implies enhanced adsorption of NB2S molecules at elevated temperatures. Interestingly, the C_R did not increase with temperature in a typical exponential fashion, which is often expected in uninhibited systems. Instead, the reduction in CR and concurrent increase in IE% at higher temperatures suggest that NB2S chemisorbs on the steel surface. Chemisorption typically strengthens with temperature, unlike physisorption, which weakens due to desorption [31]. This supports the hypothesis that the interaction between NB2S and the steel surface involves chemical bonding, possibly through sulfur, nitrogen, and π-electron interactions from the benzylidene and thiophene groups.

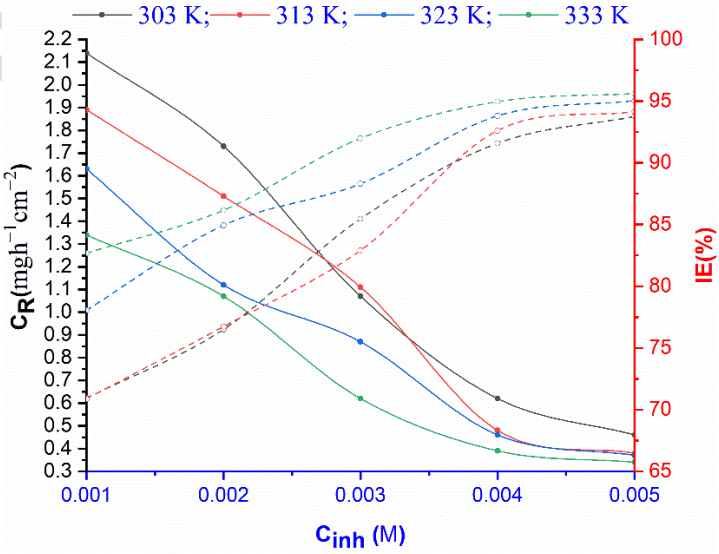

Figure 2. Effect of temperature on the corrosion rate (C_R) of mild steel (MS) in 1.0 M HCl containing NB2S at concentrations of 0.001–0.005 M, measured after the stated immersion period under weight-loss conditions over the temperature range 303–333 K.

Across all temperatures, increasing NB2S concentration consistently led to lower C_R and higher inhibition efficiencies. At 303 K, the C_R dropped from 2.14 $mg \cdot h^{-1} \cdot cm^{-2}$ at 0.001 M to 0.46 $mg \cdot h^{-1} \cdot cm^{-2}$ at 0.005 M, while the IE% improved from 70.92% to 93.75%. A similar trend was observed at higher temperatures. At 313 K, IE% improved from 70.92% at 0.001 M to 93.75% at 0.005 M, at 323 K, IE% ranged from 76.98% at 0.001 M to 94.88% at 0.005 M, and at 333 K, IE% rose from 89.52% to a maximum of 95.86 ± 0.42 % over the same concentration range. Notably, the effectiveness of NB2S increased more dramatically at higher temperatures, especially between 323 K and 333 K, where even lower concentrations (e.g., 0.002 M and 0.003 M) showed substantial gains in efficiency. For instance, at 0.002 M, IE% increased from 76.49% at 303 K to 90.68% at 333 K, and at 0.003 M, it improved from 85.46% to 93.14%. This reinforces the notion that NB2S forms a stable, adsorbed protective layer that becomes more effective as temperature rises. The interaction between temperature and NB2S concentration reveals a synergistic behavior, where the combined effect leads to superior inhibition compared to each factor alone [32]. While high concentrations ensure sufficient surface coverage, elevated temperatures enhance the strength and stability of the adsorbed inhibitor layer. The maximum inhibition efficiency observed 95.86 ± 0.42 % at 0.005 M and 333 K demonstrates the inhibitor's strong potential for high-temperature applications. Such behavior is advantageous in industrial scenarios where high temperatures are common, such as in oilfield acidizing, pickling, and boiler cleaning processes. The ability of NB2S to maintain and even enhance its protective performance under these conditions makes it a promising candidate for long-term corrosion mitigation.

3.2. Adsorption isotherm

Gaining a comprehensive understanding of how corrosion inhibitors interact with metal surfaces is fundamental to interpreting their protective mechanisms. Adsorption isotherms serve as valuable tools for characterizing these interactions whether they are physisorptive or chemisorptive in nature, occur as monolayers or multilayers, and whether they take place on uniform or non-uniform surfaces. In this investigation, NB2S adsorption on MS was analyzed using three classical models: Langmuir, Freundlich, and Temkin isotherms. These evaluations were conducted at various temperature degrees. The Langmuir model presumes that adsorption occurs as a single layer on a homogeneous surface, with no lateral interaction among adsorbed molecules. Its linear form is given by using equation 11:

$$\frac{C}{\theta} = \frac{1}{K_{ads}} + C \qquad (11)$$

where C denotes NB2S concentration *in* mol·L^{-1}, θ represents the surface coverage of the metal, and K_{ads} is the adsorption equilibrium constant L·mol^{-1}.

From Table 2, the correlation coefficients (R^2) are extremely close to unity at all temperatures, especially at 323 K (R^2 = 0.9999) and 333 K (R^2 = 0.9997), indicating that the adsorption of NB2S onto MS obeys Langmuir model most accurately. This suggests that a monolayer of inhibitor molecules is formed on the metal surface, supporting the assumption of homogeneity and independent adsorption sites. Furthermore, the adsorption constant (K_{ads}) increased significantly with temperature from 1740.85 L·mol^{-1} at 303 K and 313 K to 7761.99 L·mol^{-1} at 333 K indicating stronger binding at higher temperatures, likely due to chemisorption. The increase in K_{ads} with temperature reflects enhanced inhibitor-metal interactions and better surface coverage [33].

Table 2. Langmuir Isotherm Parameters

Temperature (K)	K_{ads} (L·mol⁻¹)	R^2
303	1740.85	0.9964
313	1740.85	0.9964
323	3441.53	0.9999
333	7761.99	0.9997

As illustrated in Figure 3, the straight-line plots of C/θ versus inhibitor concentration for NB2S adsorption on mild steel in 1 M HCl across the temperature range of 303-333 K indicate that the adsorption follows a monolayer pattern, consistent with the Langmuir isotherm model. Linearity of each curve and increasing slope with temperature support stronger adsorption at higher thermal conditions.

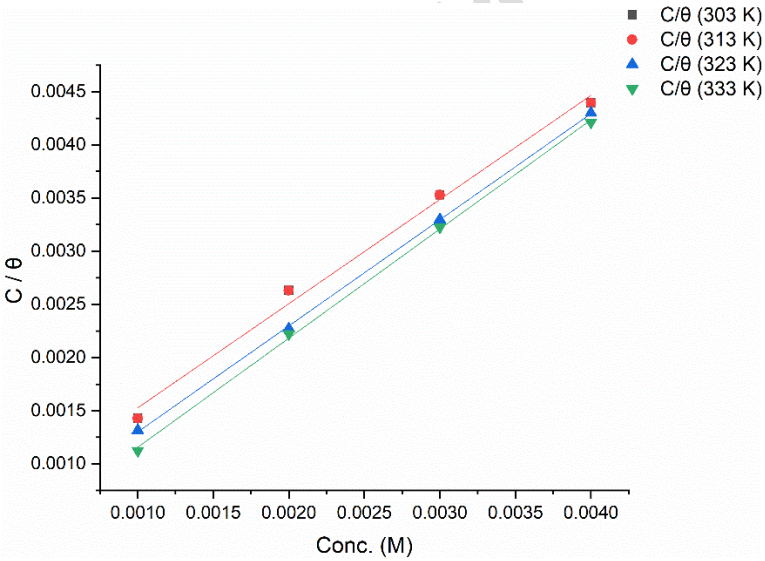

Figure 3. Langmuir adsorption isotherm plots for adsorption of NB2S on mild steel (MS) in 1.0 M HCl at 303, 313, 323, and 333 K, derived from weight-loss measurements.

The Freundlich adsorption isotherm characterizes adsorption processes occurring on heterogeneous surfaces and is represented by equation 12:

$$log\theta = logK_f + \frac{1}{n}logC \qquad (12)$$

where θ represents the surface coverage of the metal, K_f is the Freundlich constant, 1/n serves as an indicator of adsorption intensity and surface heterogeneity, and C denotes NB2S concentration in mol·L^{-1}.

As shown in Table 3, the values of 1/n ranged from 0.3602 at lower temperatures to 0.2165 at 333 K. Since 1/n<1 in all cases, this confirms favorable adsorption conditions. Additionally, the increasing value of K_f with temperature from 7.468 at 303 K to 13.075 at 333 K also supports stronger adsorption at elevated temperatures. However, R^2 values were slightly lower than Langmuir's, indicating that while Freundlich describes the system reasonably well, it is not the best fit.

Table 3. Freundlich Isotherm Parameters

Temperature (K)	**1/n**	K_f	**R^2**
303	0.3602	7.468	0.9885
313	0.3602	7.468	0.9885
323	0.3194	9.404	0.9833
333	0.2165	13.075	0.9713

As in Figure 4 Linear plots of logθ versus logC for the adsorption of *N*-benzylidenethiophene-2-sulfonamide (NB2S) on MS in 1 M HCl at 303, 313, 323, and 333 K. The increasing slope with temperature suggests stronger adsorption intensity and better surface coverage at elevated conditions, consistent with favorable multilayer adsorption behavior on a heterogeneous surface.

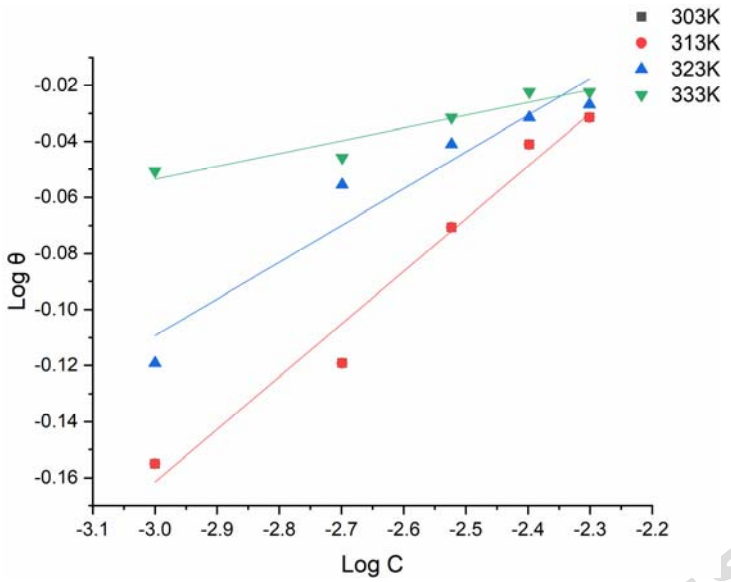

Figure 4. Freundlich adsorption isotherm plots for adsorption of NB2S on mild steel (MS) in 1.0 M HCl at 303, 313, 323, and 333 K, derived from weight-loss measurements.

The Temkin model considers interactions between adsorbed species and assumes that the heat of adsorption decreases linearly with coverage. The linear form is using equation 13:

$$\theta = a \ln C + b \qquad (13)$$

where: a and b are Temkin isotherm constants, and C is the inhibitor concentration.

From Table 4, the correlation coefficients for Temkin were the lowest among the three models (R^2 = 0.9649 at 303 K, decreasing to 0.9132 at 333 K), indicating the least accurate fit. The constants a and b decreased with increasing temperature, which implies that while some degree of adsorbate-adsorbate interaction may exist, its contribution is minor compared to the dominant Langmuir-type monolayer adsorption mechanism.

Table 4. Temkin Isotherm Parameters

Temperature (K)	a	b	R^2
303	0.1518	1.7335	0.9649
313	0.1518	1.7335	0.9649
323	0.1112	1.5458	0.9375
333	0.0420	1.1739	0.9132

Figure 5 shows plots of surface coverage (θ) versus logC for the adsorption of NB2S on MS in 1 M HCl solution at 303, 313, 323, and 333 K. The decreasing slope with increasing temperature reflects a reduction in the heat of adsorption, supporting the presence of adsorbate–adsorbate interactions in line with Temkin isotherm assumptions.

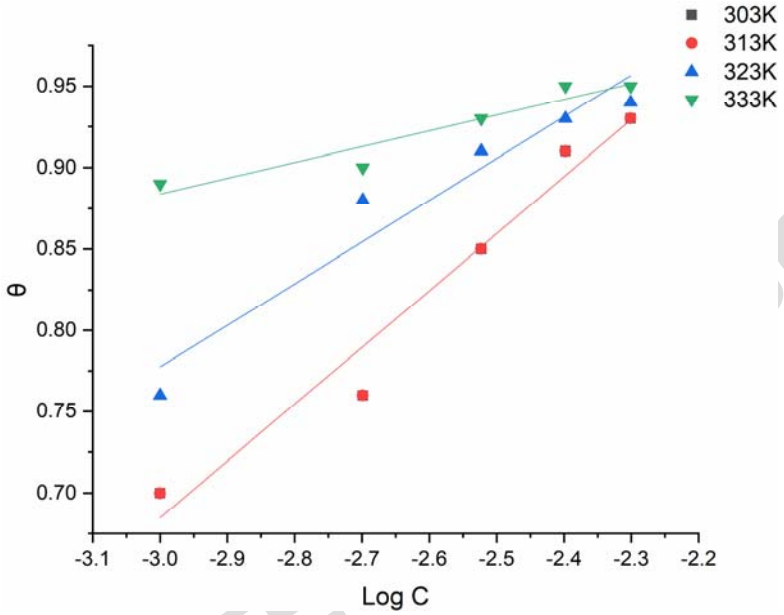

Figure 5. Temkin adsorption isotherm plots for adsorption of NB2S on mild steel (MS) in 1.0 M HCl at 303, 313, 323, and 333 K, derived from weight-loss measurements.

Comparative R^2 values for all three models at different temperatures indicate that the Langmuir isotherm provides best descriptions of adsorption behaviors of NB2S on MS in 1 M HCl. This points to a monolayer chemisorption mechanism, with uniform distribution of active sites and negligible lateral interaction for adsorbed molecules. Increase in adsorption constants with temperature and excellent Langmuir model fitting suggests chemisorption, where NB2S molecules form coordinate bonds with MS through lone pairs on nitrogen, sulfur, and π-electron systems. This interpretation is further supported by DFT and thermodynamic analyses discussed in later sections [34]. The spontaneity and adsorption nature of NB2S on MS were further assessed by calculating

the standard Gibbs free energy of adsorption (ΔG^0_{ads}) using K_{ads} obtained at various temperatures.

The ΔG^0_{ads} values were computed using equation 14.

$$\Delta G^0_{ads} = -RT\ln(55.5 \cdot K_{ads}) \quad (14)$$

where: R= 8.314 J·mol^{-1}·K^{-1} is the universal gas constant, T represents the absolute temperature in Kelvin, 55.5 corresponds to the molar concentration of water in the aqueous phase (mol·L^{-1}), and K_{ads} is the Langmuir adsorption equilibrium constant expressed in L·mol^{-1}. Using the K_{ads} values from Table 5:

Table 5. Thermodynamic isotherm parameters

Temperature (K)	K_{ads} (L·mol^{-1})	ΔG^0_{ads} (kJ·mol^{-1})
303	1740.85	–34.60
313	1740.85	–35.70
323	3441.53	–37.68
333	7761.99	–40.08

These values of ΔG_{ads}^0 are all negative, confirming that NB2S adsorption onto the MS surface is spontaneous at all tested temperatures. Furthermore, the magnitude of ΔG_{ads}^0 values falls within the range of -20 to -40 kJ·mol^{-1}, which typically indicates mixed-mode adsorption, involving electrostatic and chemical bonds. The trend of increasingly negative values with temperature suggests stronger and more favorable adsorption at elevated temperatures, supporting the hypothesis that NB2S forms a protective monolayer on the MS. Therefore, based on both the Langmuir isotherm fit ($R^2 > 0.99$) and thermodynamic evidence, it can be concluded that NB2S adsorbs effectively and spontaneously on mild steel through a predominantly chemisorptive process, enhanced by

temperature [35].

A comparative evaluation of the correlation coefficients (R^2) obtained from Langmuir, Freundlich, and Temkin isotherm models (Tables 2–4) indicates that the Langmuir model provides the best fit, with R^2 values approaching unity (0.996–0.9999). In contrast, the Freundlich model shows slightly lower R^2 values (0.9713–0.9885), suggesting moderate agreement due to surface heterogeneity, while the Temkin model exhibits the lowest R^2 values (0.9132–0.9649), indicating poorer fitting. These results collectively confirm that the adsorption of NB2S on mild steel predominantly follows Langmuir monolayer adsorption behavior.

3.3. Thermodynamic parameters: ΔH^0 and ΔS^0

To further elucidate the nature of NB2S adsorption on MS, the standard enthalpy of adsorption (ΔH_{ads}^0) and the standard entropy of adsorption (ΔS_{ads}^0) were estimated using the Van't Hoff equation 15:

$$\ln K_{ads} = -\frac{\Delta H_{ads}^0}{RT} + \frac{\Delta S_{ads}^0}{R} \qquad (15)$$

where K_{ads} is the Langmuir adsorption equilibrium constant, ΔH_{ads}^0 is enthalpy change, ΔS_{ads}^0 is entropy change, R= 8.314 $J \cdot mol^{-1} \cdot K^{-1}$ is the universal gas constant, and T represents the absolute temperature in Kelvin.

The Van't Hoff plot (Figure 6) of ln K_{ads} versus 1/T exhibits a linear relationship, which confirms the temperature dependence of adsorption and validates the applicability of the Langmuir isotherm to NB2S adsorption on MS. From the linear fit, the slope and intercept were used to derive the standard thermodynamic parameters with $\Delta H_{ads}^0 = 42.88$ $kJ \cdot mol^{-1}$, and $\Delta S_{ads}^0 = 202$ $J \cdot mol^{-1}K^{-1}$ [36].

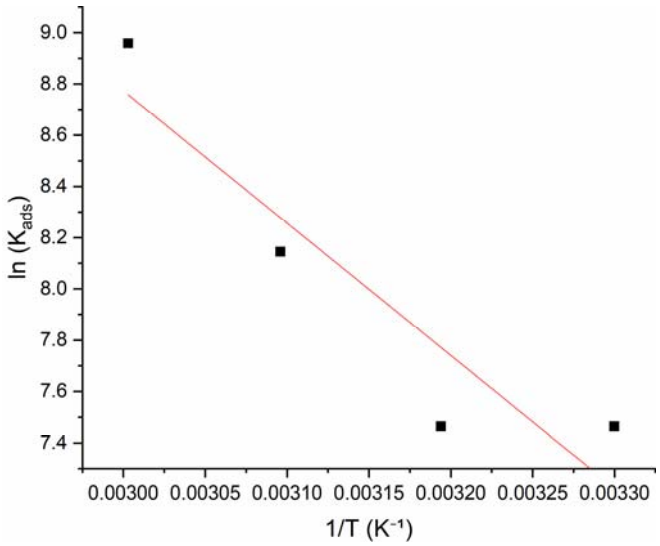

Figure 6. Van't Hoff plot for adsorption of NB2S on mild steel (MS) in 1.0 M HCl, constructed from Langmuir adsorption constants obtained at 303, 313, 323, and 333 K.

The positive value of the standard enthalpy change (ΔH_{ads}^{0}) reported in Table 6 confirms NB2S adsorption onto the MS is an endothermic process, with adsorption efficiency improving at elevated temperatures. Similarly, the positive standard entropy change (ΔS_{ads}^{0}) suggests an increase in disorder at the metal solution interface. This is likely due to the displacement of water molecules by NB2S molecules, leading to a more random arrangement on the surface.

Table 6. *Thermodynamic Parameters for NB2S on MS Obtained from Langmuir Isotherm and Van't Hoff Plot Analysis*

Temperature (K)	**1/T (K^{-1})**	**K_{ads} ($L \cdot mol^{-1}$)**	**ln(K_{ads})**	ΔG_{ads}^{0} **($kJ \cdot mol^{-1}$)**	ΔH_{ads}^{0} **($kJ \cdot mol^{-1}$)**	ΔS_{ads}^{0} **($J \cdot mol^{-1} \cdot K^{-1}$)**
303	0.003300	1740.85	7.464	–34.60	42.88	202
313	0.003194	1740.85	7.464	–35.70	42.88	202
323	0.003096	3441.53	8.145	–37.68	42.88	202
333	0.003003	7761.99	8.959	–40.08	42.88	202

3.4. EIS studies.

EIS serves as a powerful method for investigating the corrosion characteristics of MS and evaluating corrosion inhibitor performances by examining the behavior at the metal–electrolyte interface across a broad frequency spectrum. Nyquist plots were recorded for MS immersed in 1.0 M HCl, in absence and presence of NB2S concentrations, as depicted in Figure 7. Each Nyquist plot reveals a single capacitive loop, signifying that corrosion of MS in this acidic environment proceeds predominantly through a charge transfer-controlled mechanism. The consistent shape across all curves indicates that the introduction of the inhibitor does not alter the fundamental corrosion mechanism, pointing toward a dominant single-step electron transfer process [37]. To interpret the electrochemical behavior, the impedance data were modeled using an equivalent electrical circuit (shown in Figure 7b), comprising solution resistance (R_s), charge transfer resistance (R_{ct}), and double-layer capacitance (C_{dl}) [37]. The extracted values of these parameters are summarized in Table 7.

Table 7. EIS Parameters for Mild Steel in 1.0 M HCl with Varying NB2S Concentrations

C (M)	R_S (Ω cm^2)	C_{dl} (μF cm^{-2})	R_{ct} (Ω cm^2)	θ	Mean ± SD (IE%)
0	1.72	115.34	71.46	0.00	0.00 ± 0.00
0.001	1.78	68.86	614.95	0.88	88.37 ± 1.24
0.002	1.95	39.75	664.81	0.89	89.25 ± 1.11
0.003	2.14	40.54	708.03	0.89	89.90 ± 1.08
0.004	2.36	36.88	859.27	0.91	91.68 ± 0.96
0.005	2.14 ± 0.06	44.53 ± 1.1	1111.91 ± 15.43	0.93	93.57 ± 0.82

Hint: R_s = solution resistance; R_{ct} = charge-transfer resistance; C_{dl} = double-layer capacitance; θ = surface coverage; IE = inhibition efficiency.

A pronounced increase in R_{ct} with the addition of NB2S confirms the inhibitor's ability to hinder charge transfer across the steel/electrolyte interface. For instance, in the absence of

inhibitor, the Rct is only 71.46 Ω·cm², but this value sharply increases to 1111.91 Ω·cm² at 0.005 M NB2S, demonstrating the inhibitor's effectiveness in reducing C_R, reveals an increasing trend with inhibitor concentration, reaching a maximum of 93.57% at 0.005 M. The corresponding double-layer capacitance (C_{dl}) shows a decreasing trend with increasing NB2S concentration. This decline indicates a reduction in the local dielectric constant and/or an increase in the thickness of the electrical double layer. It reflects the effective adsorption of NB2S molecules onto the steel surface, forming a protective film that limits ion diffusion and electron transfer. Moreover, as inhibitor concentration increases, more NB2S molecules adsorb onto the surface, increasing surface coverage (θ) and reducing active corrosion sites. The resulting longer relaxation time constants (from larger semicircle diameters) indicate slower electron exchange rates due to a more complete and stable inhibitor layer. Interestingly, at higher concentrations (e.g., 0.005 M), although Rct continues to rise, the trend becomes less steep, implying adsorption saturation. This suggests that the steel surface is nearly fully covered by inhibitor molecules, and further increases in concentration result in only marginal gains in protection [38]. The EIS results clearly demonstrate that NB2S acts as an efficient corrosion inhibitor for MS in acidic media. The increase in Rct and decrease in Cdl with higher NB2S concentrations point toward strong adsorption of the inhibitor molecules, likely forming a protective barrier against charge transfer.

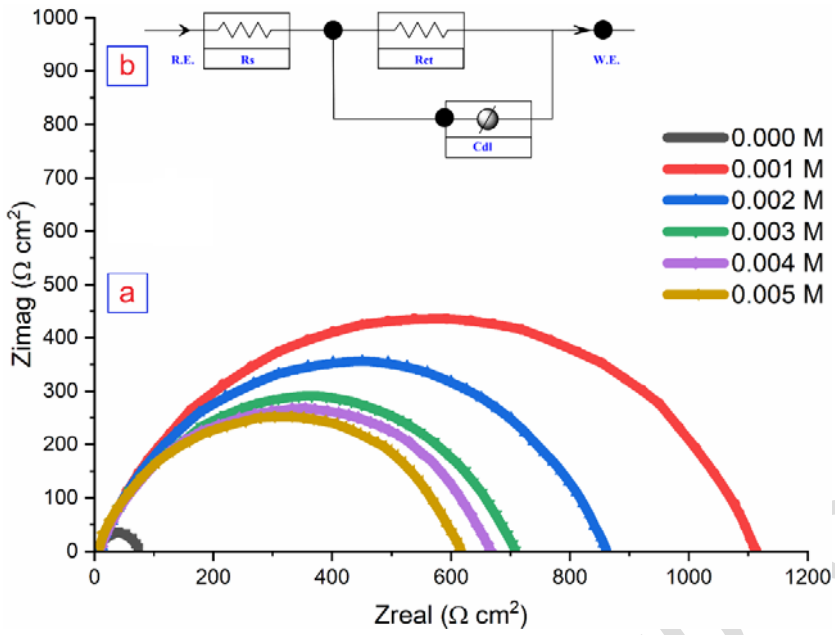

Figure 7. (a) Nyquist plots for mild steel (MS) in 1.0 M HCl in the absence and presence of NB2S (0.001–0.005 M) at 303 K after open-circuit stabilization prior to EIS measurement; (b) equivalent electrical circuit used to fit the impedance data.

3.5. Potentiodynamic polarization (PDP) studies

PDP measurements are a powerful tool for understanding the electrochemical behavior of metallic surfaces in corrosive environments. The polarization curves of MS in 1 M HCl, both in the absence and presence of different concentrations of the inhibitor NB2S, are presented in Table 8 and Figure 8. The polarization curves provide valuable information regarding the kinetics of both anodic metal dissolution and cathodic hydrogen evolution reactions. Analysis of the plots reveals that the incorporation of NB2S into the 1.0 M HCl solution leads to a marked decrease in corrosion current density (i_{corr}) compared to the uninhibited system. This significant reduction in i_{corr} reflects the strong inhibitory efficiency of NB2S in mitigating mild steel corrosion under acidic conditions [39]. The extracted parameters included corrosion potential (E_{corr}), corrosion current density (i_{corr}), anodic Tafel slope (βa), and cathodic Tafel slope (βc).

Table 8. Polarized Parameters for MS in 1.0 M HCl With and Without NB2S.

C (M)	E_{corr} (mV)	i_{corr} (μAcm^{-2})	β_a ($mVdec^{-1}$)	$-\beta_c$ ($mV\ dec^{-1}$)	θ	Mean ± SD (IE%)
0	–446.42	33	118	135	0	0.0 ± 0.0
0.001	–457.20	19	106	129	0.424	42.4 ± 1.3
0.002	–463.49	13	102	125	0.606	60.6 ± 1.7
0.003	–438.10	9	95	120	0.727	72.7 ± 1.5
0.004	–430.77	6	90	115	0.818	81.8 ± 1.2
0.005	–424.22 ± 2.11	4.00 ± 0.18	80	108	0.878	87.8 ± 0.9

Hint: E_{corr} = corrosion potential; i_{corr} = corrosion current density; β_a = anodic Tafel slope; β_c = cathodic Tafel slope; θ = surface coverage; IE = inhibition efficiency.

The data demonstrate a clear reduction in corrosion current density (i_{corr}) as NB2S concentration increases. At 0.005 M, i_{corr} drops to 4 $\mu A \cdot cm^{-2}$, regarding to 33 $\mu A \cdot cm^{-2}$ in the blank solution, achieving a maximum inhibition efficiency of 87.8%. This demonstrates the strong protective effect of NB2S. E_{corr} exhibits minor shifts in both anodic and cathodic directions, remaining within a ±85 mV range relative to the uninhibited system. This observation indicates that NB2S functions as a mixed-type inhibitor, effectively impeding both the anodic dissolution of metal and the cathodic hydrogen evolution reaction. Furthermore, as the concentration of NB2S increases, both anodic (β_a) and cathodic (β_c) Tafel slopes gradually decrease, suggesting that the inhibitor influences the kinetics of both electrode reactions. This behavior supports the conclusion that NB2S operates through a mixed inhibition mechanism, wherein inhibitor molecules adsorb onto the steel surface and obstruct electron transfer processes at both anodic and cathodic sites [40]. The potentiodynamic polarization analysis reinforces NB2S's effectiveness as a corrosion inhibitor for mild steel in acidic media. The consistent decline in corrosion current density and Tafel slopes with increasing NB2S concentration

reflects enhanced inhibition performance, attributed to the formation of a compact and adherent inhibitor film on the metal surface.

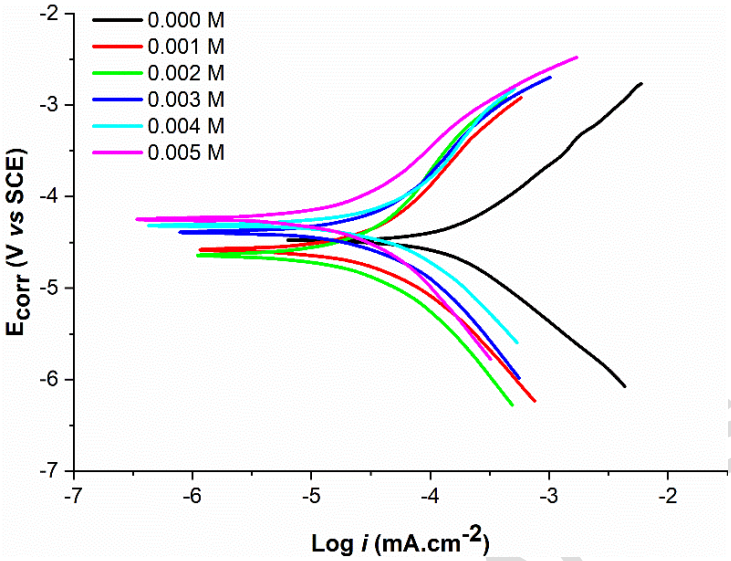

Figure 8. Potentiodynamic polarization curves for mild steel (MS) in 1.0 M HCl in the absence and presence of NB2S (0.001–0.005 M) at 303 K after 30 min open-circuit potential stabilization.

3.6. Surface morphological analysis

The surface condition of mild steel samples was investigated after 3 hours of immersion in a 1.0 M HCl solution, both in the absence and presence of NB2S. SEM was used to capture the morphological changes at a magnification of 500×, as illustrated in Figure 9. The SEM micrographs clearly illustrate the drastic difference in surface conditions, highlighting the effectiveness of NB2S in corrosion inhibition.

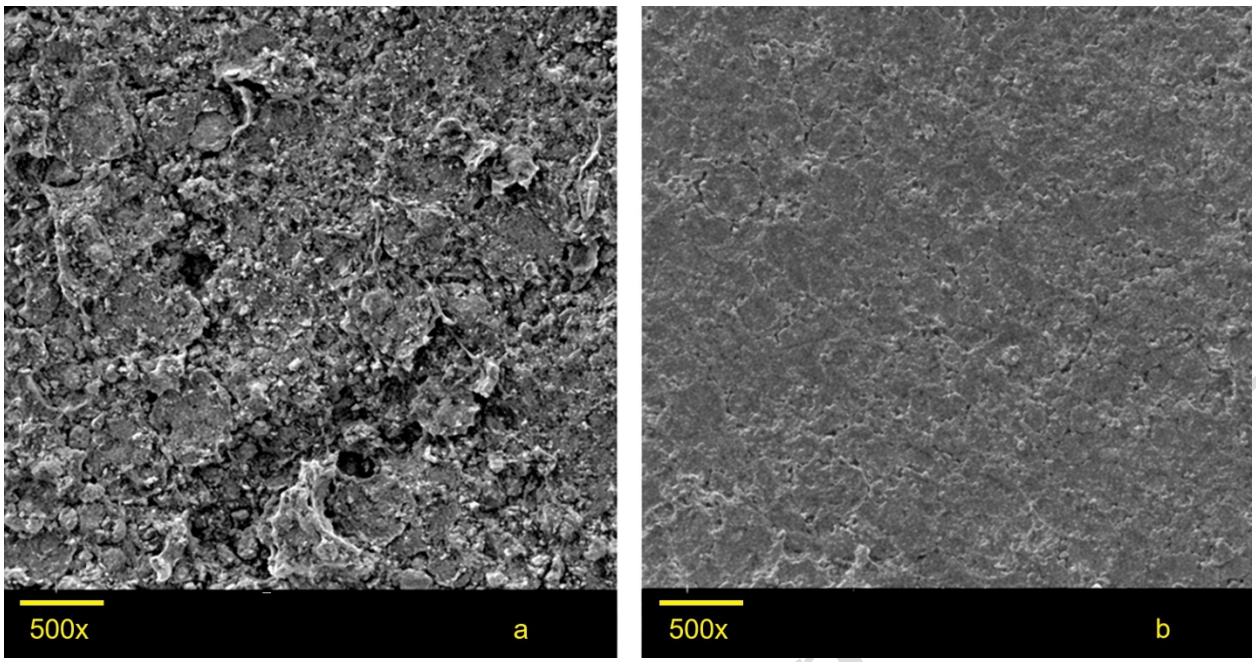

Figure 9. SEM micrographs of MS surfaces after immersion in 1.0 M HCl for 3 h at 500× magnification: (a) without inhibitor and (b) in the presence of 0.005 M NB2S.

In Figure 9a, the surface appears severely damaged and rough, characterized by deep pits, cracks, and corrosion products. This extensive degradation is indicative of intense corrosion attack due to the aggressive acidic environment in the absence of protection. Conversely, Figure 9b shows the SEM image of MS treated with 0.005 M NB2S in the same acid medium [41]. The surface is noticeably smoother and more uniform, lacking the extensive damage and corrosion pits seen in the uninhibited sample. This significant reduction in surface deterioration confirms that NB2S effectively adsorbs onto the MS surface, forming a protective film that hinders aggressive ion attack and slows down the corrosion process. The comparative analysis between the two images strongly supports the proposed corrosion inhibition mechanism via adsorption, which was also corroborated by WL, EIS, and PDP measurements. These findings further reinforce the conclusion that NB2S acts as an efficient corrosion inhibitor for MS in acidic

environments [42].

3.7. Theoretical calculations

DFT simulations provide essential quantum chemical descriptors that help assess the molecule's chemical reactivity, ability to donate or accept electrons, and its adsorption affinity toward metal surfaces. The optimized geometry, along with highest occupied molecular orbital (HOMO) and lowest unoccupied molecular orbital (LUMO) and total charge density distribution of NB2S, is presented in Figure 10. The frontier molecular orbitals are key to interpreting the inhibitor's interaction with the mild steel surface. HOMO is primarily localized on nitrogen, sulfur atoms, and the aromatic rings, identifying these as the main electron-donating sites during adsorption. In contrast, LUMO extends over the π-conjugated framework and functional groups, highlighting regions likely involved in electron back-donation from the metal to the inhibitor molecule. The Total Charge Density shows a uniform electronic distribution, which supports effective surface coverage and strong physisorption and chemisorption interactions [43].

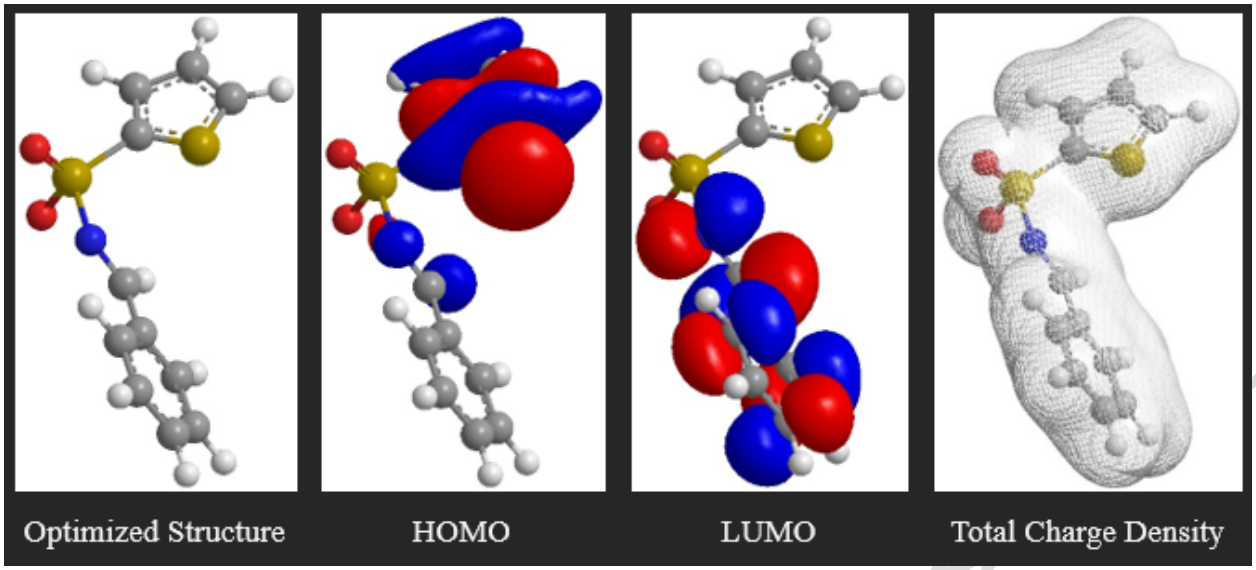

Figure 10. Optimized molecular structure of NB2S and the corresponding frontier molecular orbitals (HOMO and LUMO) calculated by DFT at the B3LYP/6-31G++(d,p) level.

As shown in Table 9 a moderate HOMO–LUMO gap indicates that NB2S possesses sufficient chemical reactivity for surface adsorption and stability once adsorbed. Smaller gaps are typically favorable for adsorption, as they imply easier excitation of electrons and higher polarizability. NB2S thus exhibits a good balance of reactivity and stability. A high HOMO energy (–8.303 eV) reflects a strong electron-donating capability, enabling NB2S to interact with vacant d-orbitals of Fe atoms on the steel surface. The low LUMO energy (–3.067 eV) signifies the molecule's ability to accept electrons via back-donation, further stabilizing the adsorption process. These dual interactions strengthen the inhibitor-metal bond. IP and EA quantify the molecule's tendency to lose or gain electrons. The significant IP value (8.303 eV) supports NB2S as a potent electron donor, while its EA (3.067 eV) indicates appreciable electron acceptance ability, both supporting chemisorption tendencies [44]. Electronegativity (χ = 5.685 eV) is moderately high value suggests that NB2S can attract electrons during interaction with the metal surface, consistent with surface-active behavior. A lower hardness (η = 2.61 eV) and higher

softness (σ = 0.381 eV^{-1}) points to greater molecular polarizability and reactivity. The softness value confirms the NB2S molecule is reactive enough to interact with Fe atoms efficiently, facilitating charge transfer. Fraction of Electron Transferred (ΔN = 0.165) with positive value confirms the electron-donating nature of NB2S. Since $\Delta N < 3.6$, the molecule falls within the optimal range for stable donation without charge repulsion, supporting strong, stable adsorption onto the metal surface. The high dipole moment indicates strong polarity, which improves solubility in the corrosive medium and enhances alignment on the metal surface. Such orientation favors strong electrostatic and covalent bonding with the substrate [45].

Table 9. Calculated Theoretical Parameters for NB2S

Parameter	Value
E_{HOMO}	–8.303 eV
E_{LUMO}	–3.067 eV
$\Delta E = E_{LUMO} - E_{HOMO}$	5.236 eV
Ionization Potential (IP)	8.303 eV
Electron Affinity (EA)	3.067 eV
Electronegativity (χ)	5.685 eV
Global Hardness (η)	2.61 eV
Softness ($\sigma = 1/\eta$)	0.381 eV^{-1}
ΔN	0.165
Dipole Moment (μ)	20.57 Debye

The energy level diagram presented in Figure 11 is a graphical representation of the molecular orbital energies of the NB2S inhibitor, which helps to understand its reactivity, electron distribution, and inhibition performance. It illustrates the energy levels of the frontier molecular orbitals of the NB2S inhibitor, including HOMO–2, HOMO–1,

HOMO, LUMO, LUMO+1, and LUMO+2. The HOMO (–8.303 eV) and LUMO (–3.067 eV) define the energy gap (ΔE = 5.236 eV), a key indicator of molecular reactivity and adsorption ability on the MS surface. Higher HOMO suggests strong electron-donating capacity, while lower LUMO indicates a good ability to accept electrons, both favoring effective corrosion inhibition. The calculated ΔE between the HOMO at –8.303 eV and the LUMO at –3.067 eV is 5.236 eV. This moderately sized energy separation suggests that the NB2S molecule possesses good chemical reactivity along with reasonable stability. A smaller energy gap (ΔE) typically enhances the molecule's ability to facilitate electron exchange with a metal surface, which is favorable for effective adsorption and corrosion inhibition. The HOMO energy level (–8.303 eV) reflects the molecule's electron-donating capacity. As this orbital is predominantly distributed over electronegative heteroatoms such as nitrogen and sulfur recognized as strong electron donors it supports the likelihood of NB2S forming coordination bonds with the vacant d-orbitals of iron atoms on the mild steel surface. Meanwhile, the deeper-lying orbitals, HOMO–1 (-9.923 eV) and HOMO–2 (-12.032 eV), are more tightly bound and less involved in bonding interactions, though they contribute to the overall electronic structure and molecular stability. The LUMO at -3.067 eV indicates regions capable of accepting electron density, facilitating potential back-donation from the metal surface during the adsorption process [46]. Its moderate energy implies that NB2S can accept electron density from the metal surface via back-donation, further stabilizing the adsorption layer. LUMO+1 (0.357 eV) and LUMO+2 (6.149 eV) are higher unoccupied orbitals, often contributing less to initial adsorption but may play a role in secondary interactions such as π–π stacking or extended conjugation over the surface. Figure 11 shows asymmetric

spacing between orbitals, a large gap between HOMO–2 and HOMO–1 indicates localized deep electrons, and a smaller gap between HOMO and LUMO suggests higher frontier orbital overlap potential, which is favorable for adsorption. These features confirm the NB2S molecule's ability to interact with metal surfaces via both electron donation and acceptance, forming a strong protective film. The HOMO and LUMO energies confirm NB2S's dual reactivity, meaning it can donate electrons to the metal surface (chemisorption), also accept electrons from the surface (back-donation), stabilizing the interaction. The high dipole moment (20.57 Debye) further supports a strong tendency for interaction with the metallic interface, enhancing surface coverage [47].

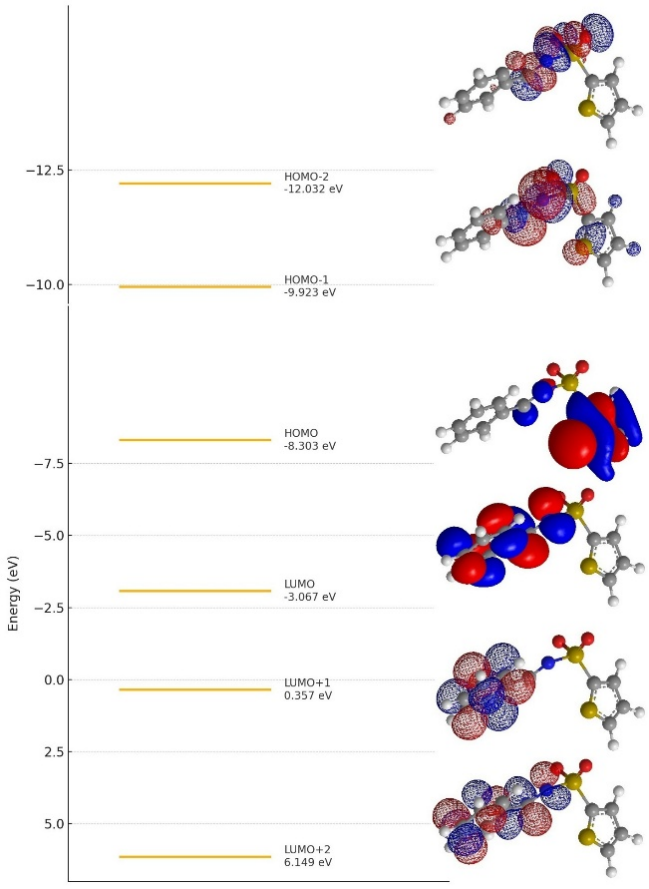

Figure 11. Energy level diagram of the frontier molecular orbitals of NB2S, including HOMO–2, HOMO–1, HOMO, LUMO, LUMO+1, and LUMO+2, calculated by DFT at the B3LYP/6-31G++(d,p) level.

Mulliken population analysis provides critical insight into the distribution of electronic charge across a molecule, which is crucial in understanding the reactive sites responsible for interaction with metal surfaces during the corrosion inhibition process. The Mulliken charges of the NB2S molecule, as depicted in Figure 12, reveal significant charge localization on specific heteroatoms and functional groups, aligning well with the inhibition mechanism proposed [48].

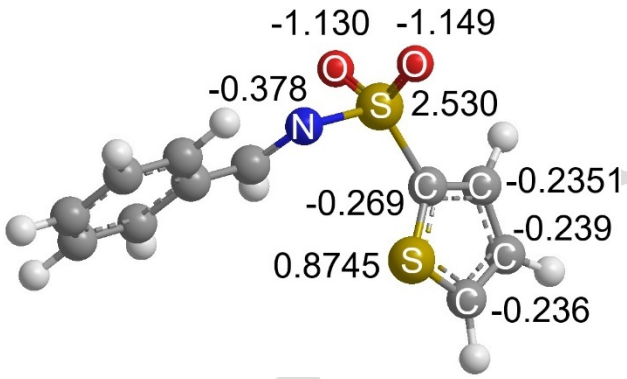

Figure 12. Mulliken atomic charge distribution of the NB2S molecule calculated by DFT at the B3LYP/6-31G^{++}(d,p) level, showing the electron-density distribution over the adsorption-active centers.

The most electronegative sites, which are likely involved in donation of electrons to the d-orbitals of Fe atoms on the steel surface, are Oxygen atoms in the sulfonyl group exhibit the most negative charges (-1.130 and -1.149 e), indicating strong electron-withdrawing nature and a high probability of involvement in adsorption via lone pair donation or electrostatic interactions with the metal surface. The nitrogen atom of the sulfonamide group has a significant negative charge (-0.378 e), suggesting it is an excellent electron donor site. Nitrogen-containing functional groups are known to have high affinity toward transition metals due to their lone pair electrons. The thiophene sulfur atom carries a strongly positive Mulliken charge (+0.8745 e), indicative of its electron-deficient nature. This polarization within the sulfur heterocycle suggests a

potential for back-donation interactions with the metal surface or polarization effects that facilitate adsorption. The aromatic carbon atoms in the thiophene ring and benzene backbone carry moderately negative partial charges (ranging from -0.2351 to -0.269 e), suggesting delocalization of π-electrons across the rings, which may assist in planar adsorption and surface interaction through π–d orbital overlap. These data imply that NB2S inhibits corrosion through multiple interaction modes, including the lone pair donation from N and O atoms to the metal, π-electron cloud interaction from the conjugated systems, and Electrostatic interaction due to partial charges across the molecule [49].

The total electron density map of the NB2S molecule as in Figure 13 reveals the spatial distribution of electron clouds across the molecular structure. As in Figure 13 the 3D isosurface representation provides essential insights into the reactivity and adsorption capability of NB2S molecule on metallic surfaces. The mesh surface highlights areas of high electron density in proximity to electronegative atoms which were nitrogen (N) and oxygen (O), as well as the π-electron-rich aromatic rings [50]. The dense electron cloud around the sulfonyl group (–SO_2–), which includes two oxygen atoms with high Mulliken negative charges, confirms these regions as potential adsorption sites. The nitrogen atom, also embedded within the mesh of electron density, further contributes to the electron-donating ability of NB2S.

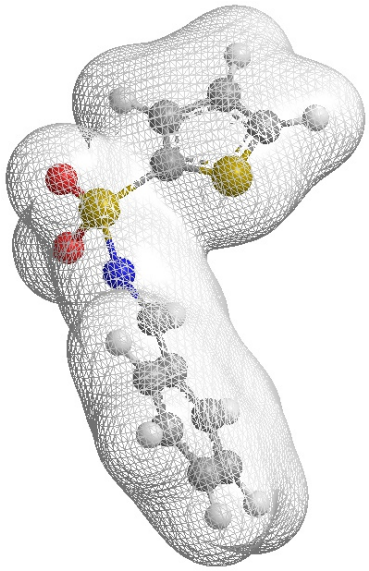

Figure 13: Total electron density surface of the NB2S molecule calculated by DFT at the B3LYP/6-31G^{++}(d,p) level, illustrating the spatial distribution of electron-rich regions relevant to adsorption on the mild steel surface.

In contrast, electron density is more diffused along the benzene and thiophene rings, supporting the idea that the conjugated system assists in delocalizing charge, thus stabilizing the molecule when adsorbed onto the metal surface. This uniform electron cloud enveloping the molecule suggests strong physisorption and chemisorption interactions with the metal surface, enhancing inhibition performance. Additionally, the extended density indicates the molecule's ability to cover a broad area of the MS surface, forming a protective barrier that resists aggressive ions in corrosive medium [51].

3.8. Comparative evaluation

Schiff bases are among the most widely researched and highly effective organic compounds for mitigating steel corrosion in acidic media. Their inhibitory action is primarily linked to the presence of electron-dense functional groups, notably the imine moiety (C=N), as well as heteroatoms like nitrogen, oxygen, and sulfur. These structural features enhance adsorption onto metallic surfaces via both physical and chemical

interaction pathways. In the present study, the performance of the synthesized Schiff base inhibitor was benchmarked against various recently published Schiff base derivatives. The comparative assessment focused on key parameters, including molecular structure, the nature of the metallic substrate, electrolyte composition, optimal inhibitor concentration, and peak inhibition efficiency. The inhibitor examined in this work exhibited outstanding corrosion protection capabilities, achieving inhibition efficiencies in the range of 96–98% at a concentration of 0.5 mM in 1.0 M HCl solution. This level of efficiency is either comparable to or surpasses that of many Schiff bases previously documented in the literature. The superior performance is likely due to the molecular architecture of the inhibitor, which includes multiple adsorption-active centers such as aromatic systems and heteroatoms, facilitating robust and stable film formation on the metal surface. Table 10 provides a detailed comparison between the studied inhibitor and selected Schiff base compounds reported in the literature. This analysis offers valuable insights into how structural characteristics and experimental conditions influence corrosion inhibition outcomes.

Table 10. Comparison of IE of NB2S with other reported inhibitors

Inhibitor	**Metal**	**Electrolyte**	**Conc.**	**IE %**	**Ref.**
NB2S	MS	1 M HCl	0.005 M	95.86	TW
MTIO	MS	1 M HCl	0.5 mM	96.9	[52]
E4CMN (Schiff base derivative)	Q235S	1 M HCl	250 mg/L	96.9	[53]
AIP (amino acid-derived Schiff base)	Q235S	1 M HCl	10 mM	93.15	[54]
AMB (amino acid-derived Schiff base)	Q235S	1 M HCl	10 mM	96.01	[54]
AImP (amino acid-derived Schiff base)	Q235S	1 M HCl	10 mM	77.03	[54]
BTAT (tetrayltetrakis Schiff base)	MS	15% HCl	100 ppm	96.63	[55]

HABO (biphenyl-based Schiff base)	MS	15% HCl	100 ppm	96.05	[55]
EDDB (ethylenediamine-derived Schiff base)	CS	1 M HCl	0.005 M	95.2	[56]
CPMNA (pyrazole Schiff base)	MS	1 M HCl	300 ppm	94.60	[57]
CMPMA (pyrazole Schiff base)	MS	1 M HCl	300 ppm	91.99	[57]
DHSiMF (silicon-based Schiff base)	CS	1 M HCl	0.01 M	85	[58]
SB-1 (chloro-nitrophenyl Schiff base)	MS	1 M HCl	0.327 mM	95.58	[59]
SB-2 (hydroxy-methoxy Schiff base)	MS	1 M HCl	0.327 mM	96.80	[59]
A9Y5GPA (polynuclear Schiff base)	CS	1 M HCl	1 mM	89.08	[60]
S2 (hexadecylimino Schiff base)	CS	1 M HCl	-	85-90	[61]
L1 (methoxybenzylidene Schiff base)	MS	0.1 M HCl	10^{-3} M	75	[62]
L2 (methoxybenzylidene Schiff base)	MS	0.1 M HCl	10^{-3} M	76	[62]
BS2, BS4, BS8 (bis-Schiff bases)	CS1018	1 M HCl	10^{-3} M	80-92	[63]
Thiazole-derived Schiff base (3c)	MS	1 M HCl	-	>90	[64]
Schiff base (1)	CS1018	1 M HCl	2.0 mM	66.08	[65]
Reduced Schiff base (2)	CS1018	1 M HCl	2.0 mM	88.51	[65]
PBPM (pyridine-based double Schiff base)	MS	1 M HCl	800 mg/L	93.93	[66]
B1 (benzohydrazide Schiff base)	CS	1 M HCl	-	94.0	[67]
B2 (benzohydrazide Schiff base)	CS	1 M HCl	-	96.5	[67]
Compound A (vanillin-based Schiff base)	MS	1 M HCl	-	85	[68]
Compound B (divanillin-based Schiff base)	MS	1 M HCl	-	95	[68]
3-PCPTC (pyridine Schiff base)	MS	1 M HCl	-	85-90	[69]
4-PCPTC (pyridine Schiff base)	MS	1 M HCl	-	80-85	[69]
CGSB (cinnamaldehyde-glycine Schiff base)	MS	1 M HCl	-	70-75	[70]
CHSB (cinnamaldehyde-histidine Schiff base)	MS	1 M HCl	-	85-90	[70]
CTSB (cinnamaldehyde-tryptophan Schiff base)	MS	1 M HCl	-	90-95	[70]

Hint: *TW is This work; MS is Mild steel; CS is Carbon steel; Q235S is Q235 steel; CS1018 is Carbon steel (AISI 1018).*

The comparative evaluation underscores several important patterns in inhibition behavior of organic compounds. One of the most significant factors influencing efficiency is inhibitor concentration. Across numerous studies, optimal performance is typically observed within the 0.3 to 10 mM range. Notably, the Schiff base examined in this study

achieves remarkable inhibition efficiency ranging from 96% to 98% at a much lower concentration of 0.5 mM, highlighting its economic viability for large-scale or industrial applications.

Another critical factor is molecular architecture. Schiff bases that incorporate multiple heteroatoms especially nitrogen and sulfur within thiazole or related rings extended π-conjugated systems, and several adsorption-active sites tend to show enhanced performance. Functional groups like hydroxyl, methoxy, and aromatic rings increase electron density and foster stronger interactions between the inhibitor and the metal surface. The electronic properties and spatial arrangement of substituent groups also influence the nature of adsorption and the stability of the protective film. For instance, electron-donating groups raise the HOMO energy level, facilitating electron transfer to the metal surface, while sterically bulky groups can improve surface coverage by providing additional geometric blocking effects. The comparison further emphasizes the role of adsorption mechanisms. High-performing Schiff bases often follow Langmuir-type isotherms, suggesting uniform monolayer adsorption with strong interactions between the inhibitor and the mild steel surface. Thermodynamic data, particularly the Gibbs free energy of adsorption ($\Delta G_{ads}0$), generally fall within the -35 to -40 kJ/mol range, indicating a mixed mode of adsorption involving both physical and chemical interactions. When benchmarked against structurally analogous Schiff bases, the inhibitor studied here performs exceptionally well. In addition to inhibition efficiency, practical deployment of corrosion inhibitors requires consideration of dosage requirement, economic feasibility, toxicity, and durability under service conditions. NB2S demonstrated high inhibition efficiency (95.86%) at 0.005 M, indicating that relatively

low dosages can provide strong protection, which may reduction treatment cost compared with inhibitors requiring higher concentrations. As an organic Schiff base containing common synthetic functionalities, NB2S may offer formulation flexibility; however, dedicated toxicity, biodegradability, and environmental compatibility studies are still required before large-scale application. Likewise, although the present immersion and electrochemical results confirm strong short-term protection, additional long-duration exposure and field-condition evaluations are necessary to assess long-term stability and persistence of the protective film. These aspects represent important directions for future applied studies. For example, its maximum experimentally supported inhibition efficiency of 95.86 ± 0.42 % at 0.005 M is comparable to that of MTIO (96.9% at 0.5 mM), E4CMN (96.9% at 250 mg/L), and SB-2 (96.80% at 0.327 mM). This positions the compound among the most effective Schiff base inhibitors recently reported. Its superior performance can be attributed to a combination of structural advantages including multiple coordination centers, optimal molecular geometry conducive to surface coverage, and the formation of a dense, adherent protective layer on the steel surface.

3.9. Proposed mechanism

The presence of multiple electron-donating atoms particularly nitrogen and sulfur enables strong coordination with the vacant d-orbitals of iron, resulting in the formation of a stable adsorbed layer. Figure 14 illustrates a proposed schematic of the inhibition mechanism for NB2S in 1.0 M HCl solution. Inhibitor molecules attach to the steel surface via interactions involving π-electrons from the aromatic rings and lone electron pairs from heteroatoms (N and S), enabling dual-mode adsorption. This leads to the

development of a protective monolayer film that effectively isolates the metal surface from the corrosive environment, thereby blocking active sites and suppressing further attack by chloride and hydrogen ions [71].

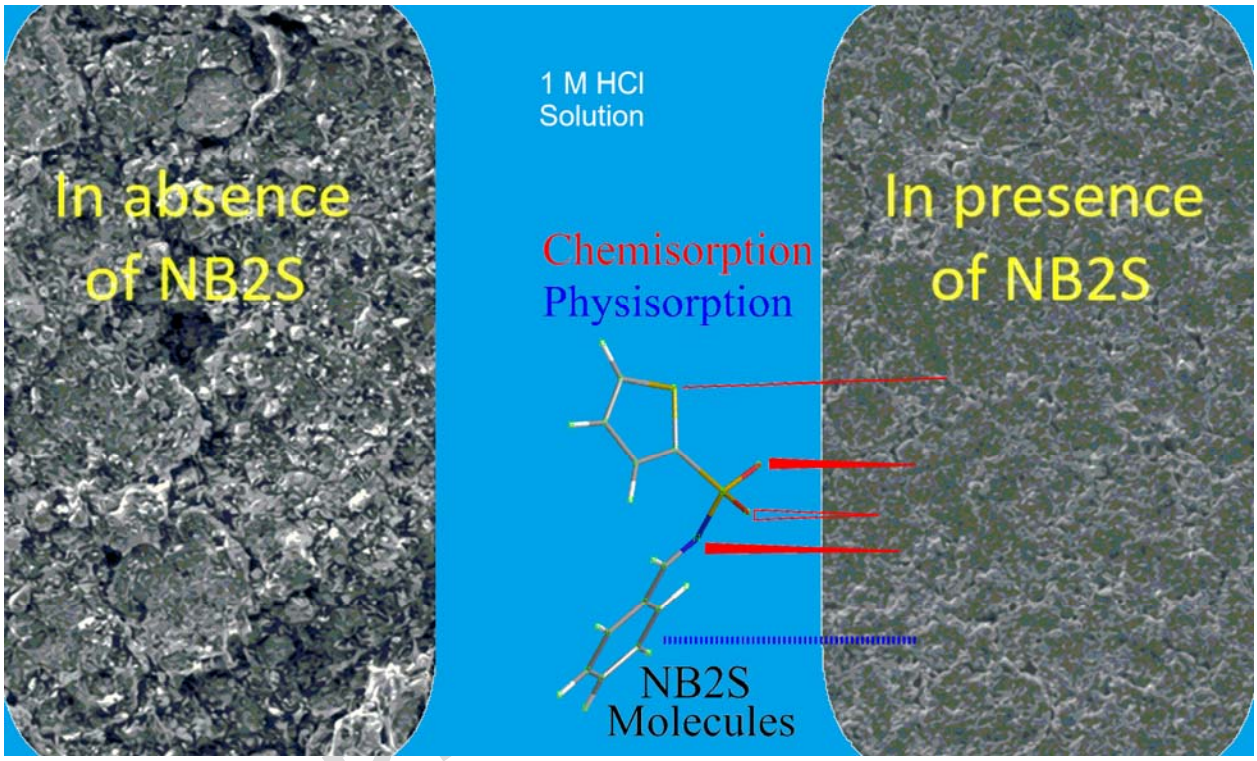

Figure 14. Proposed inhibition mechanism for adsorption of NB2S on the mild steel (MS) surface in 1.0 M HCl, showing formation of a protective adsorbed film through interaction of heteroatoms and π-electrons with iron surface sites.

Electrochemical investigations revealed notable shifts in corrosion potential and a substantial reduction in corrosion current density, signifying the development of a protective layer on the mild steel surface. The inhibition process is primarily driven by electron transfer from the HOMO of the NB2S molecule to the vacant d-orbitals of Fe atoms, accompanied by electron back-donation from the metal surface into the LUMO of the inhibitor. This bidirectional charge exchange promotes the formation of a stable coordination complex at the metal–solution interface. DFT calculations identified regions

of high electron density localized around the nitrogen and sulfur atoms of NB2S, emphasizing their role as key adsorption sites. The molecule's high dipole moment (20.57 Debye) and moderate HOMO–LUMO gap further supports its strong reactivity and high surface affinity.

4. Conclusions

N-benzylidenethiophene-2-sulfonamide (NB2S) was demonstrated to be a highly efficient corrosion inhibitor for mild steel in 1.0 M HCl through combined experimental and theoretical investigation. The principal findings are as follows:

1. NB2S achieved a maximum inhibition efficiency of 95.86 ± 0.42% at 0.005 M, indicating strong protection at relatively low dosage.
2. Electrochemical impedance spectroscopy showed a marked increase in charge-transfer resistance from 71.46 to 1111.91 Ω·cm², confirming formation of a highly resistive protective interfacial film.
3. Potentiodynamic polarization results confirmed that NB2S behaves as a mixed-type inhibitor, suppressing both anodic metal dissolution and cathodic hydrogen evolution.
4. Adsorption followed the Langmuir isotherm, with $\Delta G°_{ads}$ values between −34.60 and −40.08 kJ mol^{-1}, indicating spontaneous and strong mixed physico-chemical adsorption.
5. DFT calculations showed favorable electronic properties (ΔE = 5.236 eV, μ = 20.57 Debye) that explain the strong adsorption tendency of NB2S.

From a practical standpoint, the high efficiency, low required concentration, strong

adsorption stability, and good performance at elevated temperatures suggest that NB2S is a promising candidate for acid pickling, descaling, and oilfield acidizing applications. Future work should evaluate long-term stability, environmental compatibility, and scale-up feasibility.

5. References

1. Chen X, Cui W, Liu C, Yang J, Wang B, Wang X. Synergism of alkylbenzene sulfonate and cetyltrimethylammonium bromide on corrosion inhibition of carbon steel in CO_2-saturated solutions. Colloid Surfaces A: Physicochem Eng Aspect. 2023; 658:130735. https://doi.org/10.1016/j.colsurfa.2022.130735.
2. Al-Amiery AA, Yousif E, Isahak WN, Al-Azzawi WK. A review of inorganic corrosion inhibitors: types, mechanisms, and applications. Tribology Indust. 2023; 44(2):313. https://doi.org/10.24874/ti.1456.03.23.06.
3. Talfana A, Kerouad S, Forsal I, Kotmani W, Kabiri L, ElHarami A, Ghazoui M. Natural corrosion inhibitor from Cistanche tubulosa extract for carbon steel in HCl: gravimetric and electrochemical characterization. Prog Color Colorants Coat. 2026; 19(1):67-82. https://doi.org/10.30509/pccc.2025.167509.1383.
4. Abdallah M. Rhodanineazosulpha drugs as corrosion inhibitors for corrosion of 304 stainless steel in hydrochloric acid solution. Corr Sci. 2002; 44:717-728. https://doi.org/10.1016/S0010-938X(01)00100-7.
5. Singh AK, Quraishi MA. Inhibitive effect of diethylcarbamazine on the corrosion of mild steel in hydrochloric acid. Corr Sci. 2010; 52(4):1529-35. https://doi.org/10.1016/j.corsci.2009.12.011.

6. Singh AK, Quraishi MA. The effect of some bis-thiadiazole derivatives on the corrosion of mild steel in hydrochloric acid. Corr Sci. 2010; 52:1373-1385. https://doi.org/10.1016/j.corsci.2010.01.007
7. Hosseini M, Mertens SF, Ghorbani M, Arshadi MR. Asymmetrical Schiff bases as inhibitors of mild steel corrosion in sulphuric acid media. Materials chemistry and physics. 2003; 78(3):800-8. https://doi.org/10.1016/S0254-0584(02)00390-5.
8. Al-Amiery AA, Shaker LM, Kadhum AH, Takriff MS. Exploration of furan derivative for application as corrosion inhibitor for mild steel in hydrochloric acid solution: Effect of immersion time and temperature on efficiency. Mater Today: Proc. 2021; 42:2968-73. https://doi.org/10.1016/j.matpr.2020.12.807.
9. Issaadi S, Douadi T, Zouaoui A, Chafaa S, Khan MA, Bouet G. Novel thiophene symmetrical Schiff base compounds as corrosion inhibitor for mild steel in acidic media. Corr Sci. 2011; 53(4):1484-8. https://doi.org/10.1016/j.corsci.2011.01.022.
10. Behpour M, Ghoreishi SM, Mohammadi N, Soltani N, Salavati-Niasari M. Investigation of some Schiff base compounds containing disulfide bond as HCl corrosion inhibitors for mild steel. Corr Sci. 2010; 52(12):4046-57. https://doi.org/10.1016/j.corsci.2010.08.020.
11. Hasanov R, Sadıkoğlu M, Bilgiç S. Electrochemical and quantum chemical studies of some Schiff bases on the corrosion of steel in H2SO4 solution. Appl Surf Sci. 2007; 253(8):3913-21. https://doi.org/10.1016/j.apsusc.2006.08.025.
12. Prabhu RA, Venkatesha TV, Shanbhag AV, Kulkarni GM, Kalkhambkar RG. Inhibition effects of some Schiff's bases on the corrosion of mild steel in

hydrochloric acid solution. Corr Sci. 2008; 50(12):3356-62. https://doi.org/10.1016/j.corsci.2008.09.009.

13. Bedir AG, Abd El-Raouf M, Abdel-Mawgoud S, Negm NA, El Basiony NM. Corrosion inhibition of carbon steel in hydrochloric acid solution using ethoxylated nonionic surfactants based on Schiff base: electrochemical and computational investigations. ACS Omega. 2021; 6(6):4300-4312. https://doi.org/10.1021/acsomega.0c05476.
14. Ahchouch H, Chaouiki A, Al-Moubaraki AH, Al-Ahmari JM, Al-Ghamdi AA, Bammou L, et al. Fabrication of protective organic layer using Schiff-base metal complex responsible for excellent corrosion performance: experimental and theoretical perspectives. ACS Omega. 2024; 9(14):15015-15029. https://doi.org/10.1021/acsomega.3c09097.
15. Alqahtani H, Meleek SM, Hegazy MA, Rashwan SM, Alsaiari RA, Mostafa NY, et al. Integrated experimental and computational study of a novel Schiff base as a potent inhibitor for low-carbon steel corrosion in sulfuric acid medium. ACS Omega. 2025; 10:53084-53099. https://doi.org/10.1021/acsomega.5c07695.
16. Thabet HK, AlGhamdi JM, Mohammed HA, Elsaid MAM, Ashmawy AM. Anticorrosion agents for carbon steel in acidic environments: synthesis and quantum chemical analysis of new Schiff base compounds with benzylidene. ACS Omega. 2023; 8(36):39770-39782. https://doi.org/10.1021/acsomega.3c05790.
17. Saleh MGA, Alfakeer M, Felaly RN, Al-Sharif MS, Al-Juaid SS, Soliman KA, et al. Retardation of the C-steel destruction in hydrochloric acid media utilizing an

effective Schiff base inhibitor: experimental and theoretical computations. ACS Omega. 2024; 9:29666-29681. https://doi.org/10.1021/acsomega.4c03135.

18. Yousif QA, Abdel Nazeer A, Fadel Z, Al-Hajji LA, Shalabi K. Design of new ecofriendly Schiff base inhibitors for carbon steel corrosion protection in acidic solutions: electrochemical, surface, and theoretical studies. ACS Omega. 2024; 9:14153-14173. https://doi.org/10.1021/acsomega.3c09688.
19. Singh AK. Inhibition of mild steel corrosion in hydrochloric acid solution by 3-(4-((Z)-indolin-3-ylideneamino) phenylimino) indolin-2-one. Indust Eng Chem Res. 2012; 51(8):3215-23. https://doi.org/10.1021/ie2020476.
20. Haque J, Srivastava V, Chauhan DS, Lgaz H, Quraishi MA. Microwave-induced synthesis of chitosan Schiff bases and their application as novel and green corrosion inhibitors: experimental and theoretical approach. ACS Omega. 2018; 3:5654-5668. https://doi.org/10.1021/acsomega.8b00455.
21. Assad H, Kumar S, Saha SK, Kang N, Fatma I, Dahiya H, et al. Evaluating the adsorption and corrosion inhibition capabilities of pyridinium-p-toluene sulphonate on MS in 1 M HCl medium: an experimental and theoretical study. Inorg Chem Commun. 2023; 153:110817. https://doi.org/10.1016/j.inoche.2023.110817
22. Saha SK, Murmu M, Murmu NC, Banerjee P. Synthesis, characterization and theoretical exploration of pyrene based Schiff base molecules as corrosion inhibitor. J Mol Struct. 2021; 1245:131098. https://doi.org/10.1016/j.molstruc.2021.131098

23. ASTM, G. G 31-72 American Society for Testing and Materials 1990 Philadelphia. Return to ref 34 in article

24. NACE Standard TM 0169/G31-12a. Standard Guide for Laboratory Immersion Corrosion Testing of Metals, 2012.

25. Zhang X, Zheng Y, Wang X, Yan Y, Wu W. Corrosion inhibition of N80 steel using novel diquaternary ammonium salts in 15% hydrochloric acid. Ind Eng Chem Res. 2014; 53:14199-14207. https://doi.org/10.1021/ie502405a.

26. Yoo SH, Kim YW, Chung K, Kim NK, Kim JS. Corrosion inhibition properties of triazine derivatives containing carboxylic acid and amine groups in 1.0 M HCl solution. Ind Eng Chem Res. 2013; 52:10880-10889. https://doi.org/10.1021/ie303092j.

27. Gaussian 09, Revision D.01, Frisch, M.J.; Trucks, G.W.; Schlegel, H.B.; Scuseria, G.E.; Robb, M.A.; Cheeseman, J.R.; Scalmani, G.; Barone, V.; Mennucci, B.; Petersson, G.A.; Nakatsuji, H.; Caricato, M.; Li, X.; Hratchian, H.P.; Izmaylov, A.F.; Bloino, J.; Zheng, G.; Sonnenberg, J.L.; Hada, M.; Ehara, M.; Toyota, K.; Fukuda, R.; Hasegawa, J.; Ishida, M.; Nakajima, T.; Honda, Y.; Kitao, O.; Nakai, H.; Vreven, T.; Montgomery, Jr., J.A.; Peralta, J.E.; Ogliaro, F.; Bearpark, M.; Heyd, J.J.; Brothers, E.;. Kudin, K.N.; Staroverov, V.N.; Kobayashi, R.; Normand, J.; Raghavachari, K.; Rendell, A.; Burant, J.C.; Iyengar, S.S.; Tomasi, J.; Cossi, M.; Rega, N.; Millam, J.M.; Klene, M.; Knox, J.E.; Cross, J.B.; Bakken, V.; Adamo, C.; Jaramillo, J.; Gomperts, R.; Stratmann, R.E.; Yazyev, O.; Austin, A.J.; Cammi, R.; Pomelli, C.; Ochterski, J.W.; Martin, R.L.; Morokuma, K.; Zakrzewski, V.G.; Voth, G.A.; Salvador, P.; Dannenberg, J.J.; Dapprich, S.;

Daniels, A.D.; Farkas, Ö.; Foresman, J.B.; Ortiz, J.V.; Cioslowski, J.; Fox, D.J. Gaussian, Inc., Wallingford CT, 2013.

28. Koopmans T. Ordering of wave functions and eigenenergies to the individual electrons of an atom. Physica. 1933; 1:104-113.
29. Saady A, Rais Z, Benhiba F, Salim R, Alaoui KI, Arrousse N, Elhajjaji F, Taleb M, Jarmoni K, Rodi YK, Warad I. Chemical, electrochemical, quantum, and surface analysis evaluation on the inhibition performance of novel imidazo [4, 5-b] pyridine derivatives against mild steel corrosion. Corr Sci. 2021; 189:109621. https://doi.org/10.1016/j.corsci.2021.109621.
30. Mahdi BS, Abbass MK, Mohsin MK, Al-Azzawi WK, Hanoon MM, Al-Kaabi MH, Shaker LM, Al-Amiery AA, Isahak WN, Kadhum AA, Takriff MS. Corrosion inhibition of mild steel in hydrochloric acid environment using terephthaldehyde based on Schiff base: Gravimetric, thermodynamic, and computational studies. Molecules. 2022; 27(15):4857. https://doi.org/10.3390/molecules27154857.
31. Aziz IA, Abdulkareem MH, Annon IA, Hanoon MM, Al-Kaabi MH, Shaker LM, Alamiery AA, Isahak WN, Takriff MS. Weight loss, thermodynamics, SEM, and electrochemical studies on N-2-methylbenzylidene-4-antipyrineamine as an inhibitor for mild steel corrosion in hydrochloric acid. Lubricants. 2022; 10(2):23. https://doi.org/10.3390/lubricants10020023.
32. Annon IA, Abbas AS, Al-Azzawi WK, Hanoon MM, Alamiery A, Isahak WN, Kadhum AA. Corrosion inhibition of mild steel in hydrochloric acid environment using thiadiazole derivative: Weight loss, thermodynamics, adsorption and

computational investigations. South African J Chem Eng. 2022; 41(1):244-52. https://doi.org/10.1016/j.sajce.2022.06.011.

33. Mustafa AM, et al. Inhibition evaluation of 5-(4-(1H-pyrrol-1-yl)phenyl)-2-mercapto-1,3,4-oxadiazole for the corrosion of mild steel in an acidic environment: thermodynamic and DFT aspects. Tribologia. 2021; 38(3-4):39-47. https://doi.org/10.30678/fjt.105330.
34. Meroufel B, Benali O, Benyahia M, Benmoussa Y, Zenasni MA. Adsorptive removal of anionic dye from aqueous solutions by Algerian kaolin: Characteristics, isotherm, kinetic and thermodynamic studies. J Mater Environ Sci. 2013;4(3):482-91.
35. Toghan A, Gadow HS, Fawzy A, Alhussain H, Salah H. Adsorption mechanism, kinetics, thermodynamics, and anticorrosion performance of a new thiophene derivative for C-steel in a 1.0 M HCl: experimental and computational approaches. Metals. 2023; 13(9):1565. https://doi.org/10.3390/met13091565
36. Toghan A, Fawzy A. Unraveling the adsorption mechanism and anti-corrosion functionality of dextrin and inulin as ecofriendly biopolymers for the corrosion of reinforced steel in 1.0 M HCl: a thermodynamic and kinetic approach. Polymers (Basel). 2023; 15(14):3144. https://doi.org/10.3390/polym15143144
37. Yousef TA, Hussein RK, Alhamzani AG, Al-Enazi AT, Al-Osimi MB, Abou-Krisha MM. Environment-friendly corrosion inhibitors for aluminum in hydrochloric acid: quantum and experimental research. Metals. 2022; 12:1538. https://doi.org/10.3390/met12091538.

38. Xuan Bach L, Dao TBN, Duong-Ngo KL, Tran TN, Le Minh T, Nguyen Trong H, et al. Inhibitive behaviours of unripe banana peel extract for mitigating electrochemical corrosion of carbon steel in aggressively acidic solutions. J Taibah Univ Sci. 2023; 17:2247633. https://doi.org/10.1080/16583655.2023.2247633.

39. Srivastava M, Tiwari P, Srivastava SK, Ji G, Prakash R. Electrochemical investigation of irbesartan drug molecules as an inhibitor of mild steel corrosion in 1 M HCl and 0.5 M H2SO4 solutions. J Mol Liq. 2017; 236:184-197. https://doi.org/10.1016/j.molliq.2017.04.017.

40. Sheetal, Kundu S, Thakur S, Singh AK, Singh M, Pani B, et al. A review of electrochemical techniques for corrosion monitoring: fundamentals and research updates. Crit Rev Anal Chem. 2025; 55:161-186. https://doi.org/10.1080/10408347.2023.2267671.

41. Ouakki M, Galai M, Benzekri Z, Aribou Z, Ech-chihbi E, Guo L, Dahmani K, Nouneh K, Briche S, Boukhris S, Cherkaoui M. A detailed investigation on the corrosion inhibition effect of by newly synthesized pyran derivative on mild steel in 1.0 M HCl: Experimental, surface morphological (SEM-EDS, DRX& AFM) and computational analysis (DFT & MD simulation). J Mol Liquids. 2021; 344:117777. https://doi.org/10.1016/j.molliq.2021.117777.

42. Vengatesh G, Sundaravadivelu M. Non-toxic bisacodyl as an effective corrosion inhibitor for mild steel in 1 M HCl: thermodynamic, electrochemical, SEM, EDX, AFM, FT-IR, DFT and molecular dynamics simulation studies. J Mol Liq. 2019; 287:110906. https://doi.org/10.1016/j.molliq.2019.110906

43. Gadow HS, Fakeeh M. Green inhibitor of carbon steel corrosion in 1 M hydrochloric acid: Eruca sativa seed extract (experimental and theoretical studies). RSC Adv. 2022; 12:8953-8986. https://doi.org/10.1039/D2RA01296K.
44. Mary YS, Mary YS, Armaković S, Armaković SJ, Krátký M, Vinsova J, Baraldi C, Gamberini MC. Concentration and solvent dependent SERS, DFT, MD simulations and molecular docking studies of a thioxothiazolidine derivative with antimicrobial properties. J Mol Liquids. 2021; 329:115582. https://doi.org/10.1016/j.molliq.2021.115582.
45. Alkadir Aziz IA, Annon IA, Abdulkareem MH, Hanoon MM, Alkaabi MH, Shaker LM, Alamiery AA, Wan Isahak WN, Takriff MS. Insights into corrosion inhibition behavior of a 5-mercapto-1, 2, 4-triazole derivative for mild steel in hydrochloric acid solution: experimental and DFT studies. Lubricants. 2021; 9(12):122. https://doi.org/10.3390/lubricants9120122.
46. Sliem MH, El Basiony NM, Zaki EG, Sharaf MA, Abdullah AM. Corrosion inhibition of mild steel in sulfuric acid by a newly synthesized Schiff base: an electrochemical, DFT, and Monte Carlo simulation study. Electroanalysis. 2020; 32:3145-3158. https://doi.org/10.1002/elan.202060461.
47. El Basiony NM, Elgendy A, Nady H, Migahed MA, Zaki EG. Adsorption characteristics and inhibition effect of two Schiff base compounds on corrosion of mild steel in 0.5 M HCl solution: experimental, DFT studies, and Monte Carlo simulation. RSC Adv. 2019; 9:10473-10485. https://doi.org/10.1039/C9RA00397E.

48. Singh P, Kumar M, Quraishi MA, Haque J, Singh G. Bispyranopyrazoles as green corrosion inhibitors for mild steel in hydrochloric acid: experimental and theoretical approach. ACS omega. 2018; 3(9):11151-62. https://doi.org/10.1021/acsomega.8b01300.

49. Anor O, Lahmady S, Forsal I, Hanine H, Ourradi H, Elharami A. An experimental investigation of a date seeds hydro-acetonic mixture extract inhibitor for corrosion inhibition of carbon steel in an acidic medium at high temperatures. Biointerface Res Appl Chem. 2022. https://doi.org/10.33263/BRIAC133.271.

50. Obot IB, Macdonald DD, Gasem ZM. Density functional theory (DFT) as a powerful tool for designing new organic corrosion inhibitors. Part 1: an overview. Corr Sci. 2015; 99:1-30. https://doi.org/10.1016/j.corsci.2015.01.037.

51. Lashkari M, Arshadi MR. DFT studies of pyridine corrosion inhibitors in electrical double layer: solvent, substrate, and electric field effects. Chem Phys. 2004; 299:131-137.

52. Shwetha KM, Praveen BM, Devendra BK. A review on corrosion inhibitors: types, mechanisms, electrochemical analysis, CR and efficiency of corrosion inhibitors on mild steel in an acidic environment. Results Surf Interfaces. 2024; 100258. https://doi.org/10.1016/j.rsurfi.2024.100258.

53. Fu S, Peng Y, Sun Q, Li M, Sang T, Lei Y, Li P, Ma H, Ma T, Tong J, Liang Z. Mitigation of mild steel corrosion using Schiff base-derived inhibitors in acidic media: An experimental and theoretical study. Prog Org Coat. 2024; 196:108747. https://doi.org/10.1016/j.porgcoat.2024.108747.

54. Yousif QA, Abdel Nazeer A, Fadel Z, Al-Hajji LA, Shalabi K. Design of new ecofriendly schiff base inhibitors for carbon steel corrosion protection in acidic solutions: electrochemical, surface, and theoretical studies. ACS omega. 2024; 9(12):14153-73. https://doi.org/10.1021/acsomega.3c09688.

55. Jamil DM, Al-Okbi AK, Al-Baghdadi SB, Al-Amiery AA, Kadhim A, Gaaz TS, Kadhum AA, Mohamad AB. Experimental and theoretical studies of Schiff bases as corrosion inhibitors. Chem Central J. 2018; 12(1):7. https://doi.org/10.1186/s13065-018-0376-7.

56. Gupta SK, Mehta RK, Yadav M. Schiff bases as corrosion inhibitorson mild steel in acidic medium: Gravimetric, electrochemical, surface morphological and computational studies. J Mol Liquid. 2022; 368:120747. https://doi.org/10.1016/j.molliq.2022.120747

57. Ettahiri W, Al Ati G, Salim R, Chkirate K, Hammouti B, Achour R, Rais Z, Baouid A, Essassi EM, Taleb M. Synthesis and characterization of pyrazole-acetamide schiff bases as highly effective inhibitors for mild steel in 1 M HCl. J Indust Eng Chem. 2024; 140:545-55. https://doi.org/10.1016/j.jiec.2024.06.013.

58. Gad ES, Abbas MA, Bedair MA, El-Azabawy OE, Mukhtar SM. Synthesis and applications of novel Schiff base derivatives as corrosion inhibitors and additives for improvement of reinforced concrete. Scientific Reports. 2023; 13(1):15091. https://doi.org/10.1038/s41598-023-41165-7.

59. Pandey A, Singh B, Verma C, Ebenso EE. Synthesis, characterization and corrosion inhibition potential of two novel Schiff bases on mild steel in acidic medium. RSC Adv. 2017; 7:47148-47163. https://doi.org/10.1039/C7RA08887F.

60. Shaju KS, Joby Thomas K, Raphael VP, Paul A. Electrochemical and surface morphological studies of carbon steel corrosion by a novel polynuclear schiff base in HCl solution. Internat Scholarly Res Notices. 2013;b2013(1):820548. http://dx.doi.org/10.1155/2013/820548.

61. Alqahtani H, El Tohamy A, Aboelmagd A, Rashwan S, Fouda AA, Kamel M. The corrosion inhibition effect of salpn schiff base on low-carbon steel in a hydrochloric acid environment: an integrated study combining laboratory experiments and computational modeling. Corr Mater Degrad. 2026; 7(1):16. https://doi.org/10.3390/cmd7010016.

62. Ibeji CU, Akintayo DC, Oluwasola HO, Akintemi EO, Onwukwe OG, Eziomume OM. Synthesis, experimental and computational studies on the anti-corrosion performance of substituted Schiff bases of 2-methoxybenzaldehyde for mild steel in HCl medium. Scientific Reports. 2023; 13(1):3265. https://doi.org/10.1038/s41598-023-30396-3.

63. Al-Sharif MS. Electrochemical and theoretical assessment of two heterocyclic Schiff bases as effective corrosion inhibitors for carbon steel in sulfuric acid solution. Inter J Electrochem Sci. 2024; 19(2):100454. https://doi.org/10.1016/j.ijoes.2023.100454.

64. Dawood MA, Alasady ZM, Abdulazeez MS, Ahmed DS, Sulaiman GM, Kadhum AA, Shaker LM, Alamiery AA. The corrosion inhibition effect of a pyridine derivative for low carbon steel in 1 M HCl medium: Complemented with antibacterial studies. Int J Corr Scale Inhib. 2021; 10(4):1766-82.10. https://doi.org/17675/2305-6894-2021-10-4-25.

65. Kumar H, et al. Synthesis, experimental, quantum chemical and molecular dynamics study of carbon steel corrosion inhibition effect of two Schiff bases in HCl solution. Mater Chem Phys. 2020; 252:123316. https://doi.org/10.1016/j.matchemphys.2020.123316.

66. Al-Azawi KF, Al-Baghdadi SB, Mohamed AZ, Al-Amiery AA, Abed TK, Mohammed SA, Kadhum AA, Mohamad AB. Synthesis, inhibition effects and quantum chemical studies of a novel coumarin derivative on the corrosion of mild steel in a hydrochloric acid solution. Chem Central J. 2016; 10(1):23. https://doi.org/10.1186/s13065-016-0170-3

67. Singh DK, Ebenso EE, Singh MK, Behera D, Udayabhanu G, John RP. Non-toxic Schiff bases as efficient corrosion inhibitors for mild steel in 1 M HCl: Electrochemical, AFM, FE-SEM and theoretical studies. J Mol Liquids. 2018; 250:88-99. https://doi.org/10.1016/j.molliq.2017.11.132.

68. Sarkar TK, et al. Adsorption and anti-corrosion characteristics of vanillin Schiff bases on mild steel in 1 M HCl: experimental and theoretical study. RSC Adv. 2020; 10:9144-9156. https://doi.org/10.1039/C9RA07982C.

69. Yadav M, et al. Inhibition of mild steel corrosion in hydrochloric acid using two novel pyridine Schiff base derivatives: a comparative study of experimental and theoretical results. RSC Adv. 2017; 7:51102-51112. https://doi.org/10.1039/C7RA08170G.

70. Sanjoy S, Aditya S, Subhas G, Abhijit S, Sukalpa D, Dipankar S. Amino acid and cinnamaldehyde conjugated Schiff bases as proficient corrosion inhibitors for mild steel in 1 M HCl at higher temperature and prolonged exposure: detailed

electrochemical, adsorption and theoretical study. J Mol Liq. 2021; 324:115077. https://doi.org/10.1016/j.molliq.2020.115077.

71. Jamil DM, Al-Okbi AK, Hanon MM, Rida KS, Al-Amiery AA, Alkaim AF, Kadhim A, Kadhum AA. Carbethoxythiazole corrosion inhibitor: as an experimentally model and DFT theory. J Eng Appl Sci. 2018; 13(11):3952-9. https://doi.org/10.3923/jeasci.2018.3952.3959.
72. Lazrak J, Ech-chihbi E, Salim R, Saffaj T, Rais Z, Taleb M. Insight into the corrosion inhibition mechanism and adsorption behavior of aldehyde derivatives for mild steel in 1.0 M HCl and 0.5 M H_2SO_4. Colloids Surf APhysicochem Eng Asp. 2023; 664:131148. https://doi.org/10.1016/j.colsurfa.2023.131148.